Apparatus for Measurement of Thermoelectric Properties of a Single Leg under Large Temperature Differences

H. Naithani,[1,2,a)] P. Ziolkowski,[2] and T. Dasgupta[1]

[1]*Metallurgical Engineering and Materials Science, Indian Institute of Technology Bombay, 400076, India*

[2]*German Aerospace Center (DLR) – Institute of Materials Research, Linder Höhe, D-51147 Cologne, Germany*

Thermoelectric (TE) devices operate under large temperature differences, but material property measurements are typically accomplished under small temperature differences. Because of the issues associated with forming proper contact between the test sample and the electrodes and the control of heat flux, there are very few reports on large temperature difference measurements. Therefore, practically relevant performance parameters of a device, namely, power output and efficiency, are estimated by temperature averaging of material properties, whose accuracy is rarely validated by experimental investigations. To overcome these issues, we report an apparatus that has been designed and assembled to measure the TE properties - Seebeck coefficient, electrical conductivity, thermal conductivity, and power output and efficiency of a single thermoelectric material sample over large temperature gradients. The sample holder – a unique feature of this design, lowers the contact resistance between the sample and the electrodes, allowing for more accurate estimates of the sample's properties. Measurements were performed under constant temperature differences (CTD) ranging from 50 K to 300 K with the hot side reaching 673 K on a metallized $Mg_2Si_{0.3}Sn_{0.7}$ leg synthesized in the laboratory. To simulate practical operating

[a)] **Author to whom correspondence should be addressed. Electronic mail: Harshita.Naithani@dlr.de**

conditions of a continuously loaded generator, continuous current flow measurements were also performed under large temperature differences. The temperature-averaged TE properties from standard low temperature difference measurements and the experimental TE properties agree with each other indicating that the designed setup is reliable for measuring various thermoelectric generator properties of single TE legs when subjected to temperature gradients between 50 K and 300 K.

I. INTRODUCTION

Thermoelectric (TE) devices convert heat energy into electrical energy and vice versa without any moving parts. They are noise-free, reliable and environment-friendly. However, their commercial usage is not as widespread as their advantages would suggest. This is in part due to their low efficiency[1], which is limited by the Carnot efficiency $\eta_C = (T_H - T_C)/T_H$ with T_H and T_C being the hot and the cold side temperature at the TE device. Additionally, physical properties of the TE materials limit the maximum conversion efficiency η_{MAX} by another factor which is a function of the figure of merit $zT = (\alpha^2 \cdot \sigma / \kappa) \cdot T_m$, defined with respect to the temperature interval of operation and its mean temperature $T_m = (T_H - T_C)/2$ and averaged values of the Seebeck coefficient α, and the electrical and thermal conductivity σ and κ, respectively. Without consideration of electrical and thermal contact resistances and influences of other device components TE conversion efficiency for a single leg is given by:

$$\eta_{MAX} = \frac{T_H - T_C}{T_H} \frac{\sqrt{1+zT}-1}{\sqrt{1+zT}+\frac{T_C}{T_H}} \tag{1}$$

In order to increase device efficiency efforts are concentrated at finding new materials with high zT, improving existing materials and lowering the contact resistances between the TE legs and the electrodes. All of these tasks require accurate measurements of the aforementioned TE properties. But material testing is normally done under low temperature differences of only a few K, while a device typically operates under hundreds of K temperature difference. Usually temperature averaging of material properties is used to approximate high temperature gradient properties and to conclude on effective operation parameters of TE devices by using such averages in constant property models (CPM) allowing for an analytical solution of the thermoelectric heat balance equation[2]. Depending on the method of averaging it is possible to get different values for the same property because material properties are functions of temperature. This makes it difficult to choose the best method although attempts have been made[3-5] to make theoretical averaging more accurate. However, experimental verification of results obtained from averaging methods is missing due to the lack of equipment capable of performing high temperature gradient characterization on materials. The need for such measurements becomes especially critical because good TE materials are identified on the basis of maximum zT, which given its low temperature gradient nature of measurement and estimation is not sufficient to determine the goodness of a TE material in practical applications.

One major issue associated with measuring the electrical and thermal signals accurately at the sample at high temperatures is creating minimally invasive thermal and electrical contacts between the sample and measurement probes. Generally, measurements on TE modules under large temperature gradients are performed with the electrical connections soldered onto the cold side. But single leg measurements require the measuring probes to be on either side of the leg and at high temperatures a generic solder simply will not hold up. While a two-point probing configuration[6] for tapping of electric signals requires low contact resistance so that the properties being measured are close to the material properties, four-point probing methods[7] can be applied to overcome the influence of electric contact resistances on measured properties. Another problem associated with large temperature gradient measurements is the cold finger effect[8, 9], which creates a temperature gradient across the thermocouple tip-sample interface and typically results in an underestimation of the temperature difference measured across a TE material leading to an overestimation of the measured Seebeck coefficient. The origin of the cold finger effect is given by an asymmetric parasitic heat flow across the sensor-sample interface. This heat flow scales with the temperature difference between the sensing point and the background temperature of signal leads. The temperature difference measurement is principally not affected by the cold finger effect, as long as the associated temperature drop is equal for all sensor interfaces. Due to similar temperatures at sensing points this can be controlled for small thermal gradient experiments to a certain extent by sophisticated constructions for sample holders involving a thermal anchorage of sensing leads. Characterization of TE materials at high thermal gradient inherently involves a higher asymmetry of temperature differences along the sensing leads and therefore can yield to a potentially increased impact of the cold finger effect [9, 10]. The measurement of the thermal conductivity is affected by the accuracy of temperature measurements likewise. Besides the cold finger effect, measurements of the thermal conductivity suffer from parasitic heat losses along the measurement configuration, which scale with the temperature difference between the sample and its surrounding, effectively impeding a precise characterization at elevated temperatures.

Experimental setups, which have tested[11, 12] bismuth telluride legs, have been reported with maximum temperature difference in the 150 K-160 K range. Zhu and Ren [13] have designed a setup, employing the four probe technique, in which the electrodes are mechanically pressed onto the single leg thereby bypassing the need to form bonded contacts, and reported measurements with a temperature difference of ~420 K. However, they perform power output and heat flow measurements separately, i.e. heat flow measurements are performed without the electrodes. Thus, power output and efficiency are measured under different conditions. Also, it must be noted that any practical application will need contacted TE legs. Thus, a setup which tests contacted legs is advantageous for a realistic prediction of performance under application-oriented conditions. As a corollary, the setup can also be used while developing contacts for various TE materials as the contact resistance can be characterized using this setup (with appropriate reference data for the electric conductivity of the employed TE material). Additionally, measurement on a contacted leg can provide more realistic input for Finite Element Method (FEM) simulations of modules.

In this work, an experimental setup has been designed and assembled which has been tested for a temperature difference of ~300 K with the hot side reaching ~673 K. The setup measures all relevant TE material properties- α, σ, κ, and the power output (P_{out}) and efficiency (η) under large temperature gradients. A novel feature of the design is the sample holder which does not require soldering of the electrodes, but can be used for testing of contacted legs at high temperatures and allows for simultaneous measurements of electrical properties and heat flow.

Testing was carried on a metallized n-type $Mg_2Si_{0.3}Sn_{0.7}$ (Bi-doped) which is a low cost, environment-friendly and high *zT* TE material[14-16]. To simulate practical working conditions steady state and transient measurements of power output and efficiency were carried out. Reference values for measurands have been calculated from temperature averaging of TE material properties, which were obtained from standard low temperature gradient measurements. The investigation reveals a good agreement between the reference and experimental values measured under large temperature gradients.

II. EXPERIMENTAL SECTION

A. Design of the Experimental Setup

A schematic of the testing assembly is shown in Figure 1. An enclosed setup was designed to conduct measurements under vacuum conditions in order to protect the sample and the components against oxidization at high temperatures. A custom-made heating block has been used as the heat source which is connected to a proportional–integral–derivative (PID) temperature controller. Two reference blocks hold the sample in between. Each block is equipped with three thermocouples, which are placed inside holes, which have a spacing of ~10 mm between each other in the direction of heat flow. All thermocouples used were class 1 type K thermocouples since they are suitable for measuring temperatures in the desired range (20°C- 500°C). These thermocouples allow for temperature measurements along the center line of each block to calculate the temperature gradient for determination of heat flow. Including the two thermocouples placed in the sample holder, a total of eight thermocouples are used. Both blocks have been manufactured with a cross section of ~10 ×10 mm^2, offering similar lateral dimensions as the sample holder. With regard to a desirably maximized applicable hot side temperature of the sample, Ni was chosen to provide a thermal connection between the heater and TE sample. A moderately high thermal conductivity (~ 90 W/mK) of the Ni block is high enough to avoid too high requirements on the heating power and thermomechanical stability of the heater. However, the temperature profile of the Ni block is almost flat rendering it unsuitable for measuring the heat flow through the sample. Therefore, reference block at the cold side of the configuration was made from stainless steel (SS 304) with a lower thermal conductivity of ~14 W/mK at room temperature[17]. In view of a limited cooling capacity of the used chiller, which improves at increased working temperatures of the coolant, the higher thermal resistance of the SS increases the temperature gradient over this block (temperatures can be recorded within the precision limits of the thermocouples used), allowing for precise heat flow measurements, but at the expense of an increased minimum cold side temperature at the sample. The bottom of the cold side block is connected to a copper cooling plate, which is cooled by the external chiller to maintain a low temperature of 293 K for all measurements. Graphite sheets are inserted between the hot side reference block and the sample holder to establish good thermal contact between these components whereas thermal paste is used between the sample holder and the cold side reference block. To minimize heat loss, reference blocks and the sample are encapsulated with ceramic wool for thermal damming.

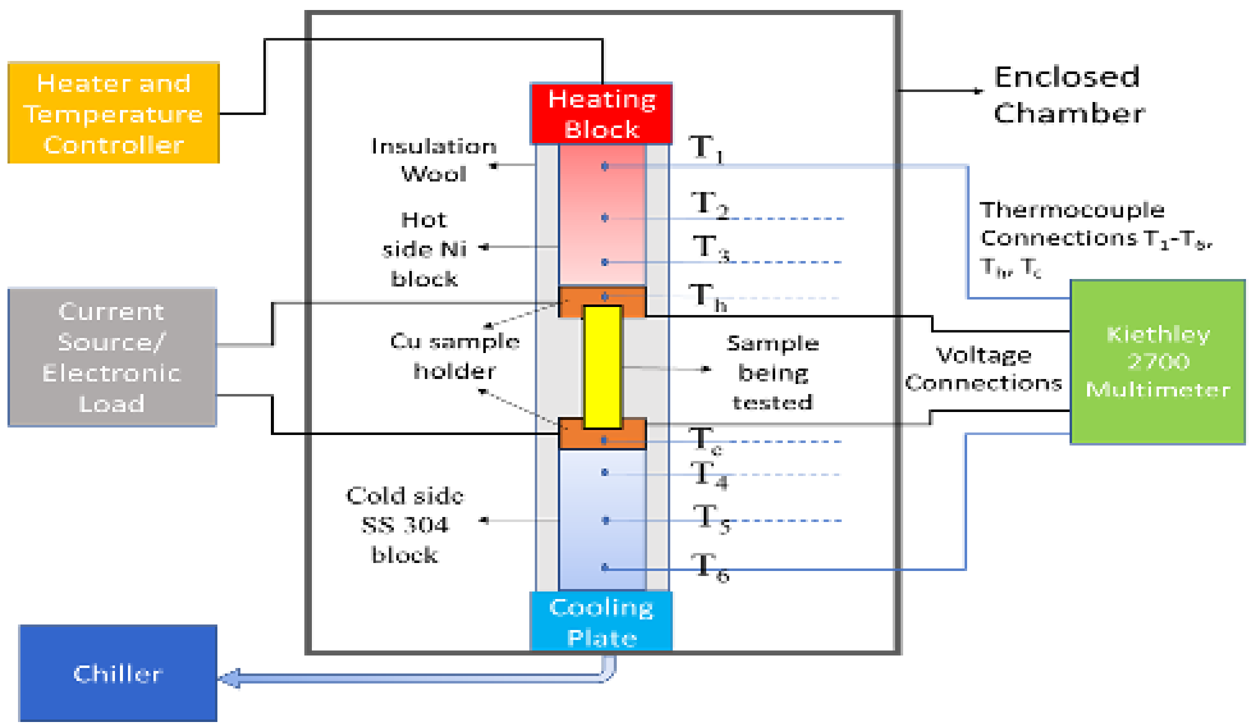

Figure 1 Schematic of the testing assembly showing the placement of the sample in the sample holder between two reference blocks with all signal connections

Temperature and voltage measurements are carried out using a 6½ digit multimeter (Keithley 2700) equipped with a scanner card (Keithley 7700). An electronic load/precision current source (GWINSTEK PPH-1503) was used for the control of the electric current through the sample. The

I-*V* measurement is based on a four-point probing configuration with individual leads for current supply (*I*) and voltage measurement (*V*). These leads are attached to the sample holder, which is a unique feature of this setup and is shown in Figure 2.

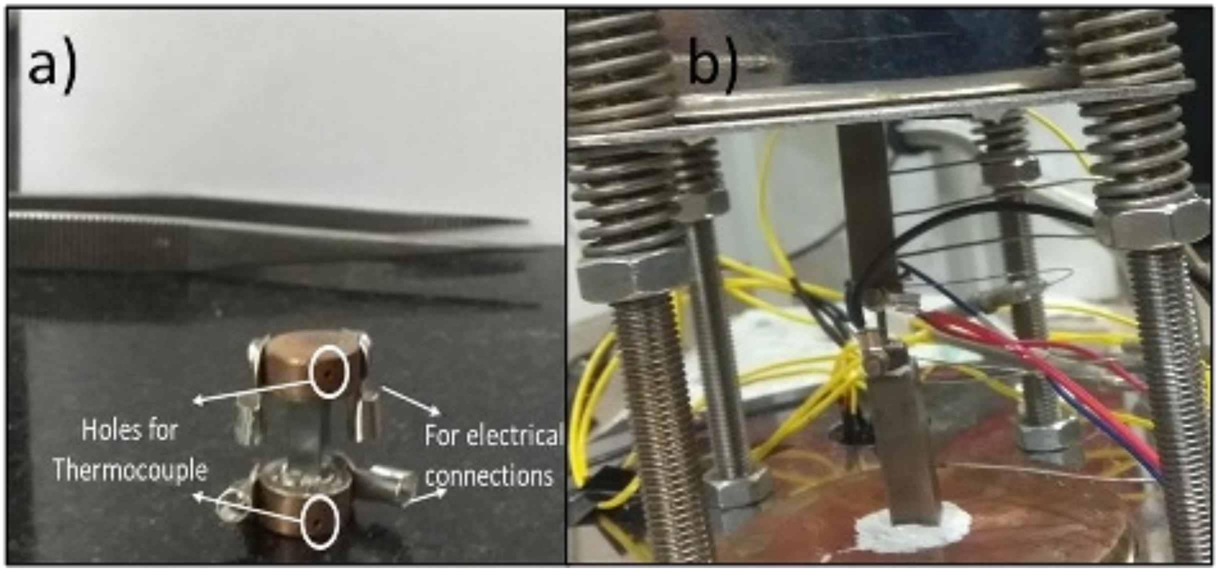

Figure 2 (a) Sample holder with the sample attached to it. The four silver colored protrusions are the lugs screwed to the holder. The white circles highlight the holes drilled for thermocouple attachment. (b) Photograph of the sample installed in the testing facility.

Being made of copper, which possesses high thermal and electrical conductivity, the sample holder does not significantly disturb the electrical and thermal field distributions within the measurement configuration. This yields low drops of temperatures and electric potentials over the sample holder, effectively increasing the signal contribution of the sample. Two holes were drilled on either side of the sample holder for thermocouple placement. Temperatures measured by these thermocouples were taken as the sample hot (T_h) and cold side (T_c) temperatures. Four more threaded holes were drilled (two on either side) and four metallic lugs were screwed to the sample holder, as shown in Figure 2 (a). Connections for current supply and voltage measurements were made by crimping the wires to the lugs, effectively establishing a four-point measurement scheme for determination of the sample voltage. This four-point measurement is neither influenced by contact resistances nor by Ohmic voltage contributions of the current-supplying leads. Copper (Cu) wires were used for voltage measurement. The low Seebeck coefficient of Cu promotes an accurate measurement of the sample's Seebeck coefficient due to low thermovoltage contributions, which are calculated from measurements of T_h, and T_c, respectively, the base temperature of the wires and their Seebeck coefficient. This allows for a correction of parasitic signal contributions from the used wiring. A photograph of the setup is shown in Figure 2 (b).

B. Material Synthesis

An ingot of nominal composition of $Mg_{2.2}(Si_{0.3}Sn_{0.7})_{0.9927}Bi_{0.0073}$ was synthesized by melting the constituent elements in an atmosphere-controlled induction melting furnace. Various elements were taken in the correct stoichiometry in a graphite crucible for melting. The melting was carried out at a furnace temperature of 1273 K in an Argon atmosphere (0.5 atm) with a holding time of 5 minutes. Excess Mg was added to account for Mg loss due to evaporation (its boiling point being 1364 K). The weight change, which was monitored after melting in all experiments, was ~0.5%. The obtained ingot was hand-crushed to a fine powder and further compacted to form a pellet using a rapid hot-induction uniaxial press at a temperature of 923 K and pressure of 50 MPa (on the furnace). To achieve high densification, a holding time of 5 minutes at the maximum temperature was maintained. X-Ray Diffraction pattern of the leg is shown in Figure 3.

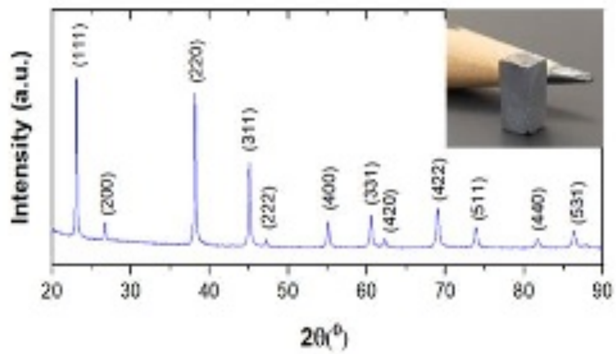

Figure 3 XRD pattern of the synthesized pellet with nominal composition of $Mg_{2.2}(Si_{0.3}Sn_{0.7})_{0.9927}Bi_{0.0073}$. The inset shows the synthesized contacted leg.

C. Joining the TE Leg to the Sample Holder

Before any connections could be made to the sample holder, the sample leg had to be attached to the sample holder. The leg (composition $Mg_{2.2}(Si_{0.3}Sn_{0.7})_{0.9927}Bi_{0.0073}$) was metallized with copper foils on both sides[18]. A mixture of powdered Ni and the TE material were placed on either side between the TE material and the Cu foils to prevent diffusion of the TE material into Cu and vice versa. This assembly was then sintered at ~923 K, using a uniaxial hot press to produce a metallized leg. To promote a good contact between the Cu sample holder and the metallized leg, Zinc was used as a high temperature solder. Zinc pieces were placed in between the metallized leg and the sample holder. This assembly was heated inside an induction furnace. Taking into consideration the melting of Zinc (693.65 K), thermal stability of the material and the temperature gradient inside the furnace, the temperature of the furnace was set to ~743 K and held for ~30 seconds. This was performed for joining both sides of the contacted leg to the sample holder, one at a time. Afterwards, the sample holder was placed inside the measurement setup and electrical and thermal connections were made.

III. PRINCIPLE OF MEASUREMENT

Two types of measurements have been performed in this study – constant temperature difference (CTD) and continuous current flow (CCF) measurements. When current is passed through the circuit, at the interface of the sample holder and TE leg, heat is released at one end and absorbed at the other due to the Peltier effect. This leads to a drop in the temperature difference across the leg and in turn in the generated thermo-voltage due to the Seebeck effect. To measure *V-I* characteristics at a *constant* temperature difference, the sequence of measurements (described in the following subsection) has been designed in a way to minimize the impact of the Peltier effect. These measurements have been referred to as the CTD measurements. The purpose of CTD measurements is to measure the TE properties under large temperature differences. The other type of measurement, i.e. the CCF measurement allows for the temperature differences to change and stabilize while the current flows through the TE leg. Thus, a single *V-I* characteristic generated during steady state measurements is associated with a varying temperature difference. The CCF measurements simulate application scenarios, as the TE generator would be under load, and are more relevant for power output and efficiency estimation. The two types of measurements are detailed in the following subsections.

A. Constant Temperature Difference (CTD) Measurements

1. Voltage and Power Output

Readings of voltage and current were taken at five different set temperatures of the heater – 373 K, 473 K, 573 K, 673 K and 763 K, while the temperature of the cooling plate was controlled by the chiller set to 293 K. The data were acquired manually. At every stabilized temperature difference, characterization started with the measurement of the open loop voltage V_{OC}. Following this, an electronic load was used to pass the desired direct current (I) through the sample. The current flow lowers the terminal voltage instantaneously by the Ohmic voltage drop over the internal resistance of the sample. Thus, immediately after activation of the current flow the voltage is noted. Secondly, due to the Peltier effect the electric current flow introduces a decrease of the temperature difference over the sample, which reduces the terminal voltage additionally. If the next V-I point had been recorded by immediately passing the next higher current value, the V-I point would have been measured at a different temperature difference. To overcome this issue, which arises due to manual data acquisition, the electronic load is switched off and the terminal voltage is allowed to return to its open circuit value due to the ceasing Peltier heat transport, which effectively yields the originally set temperature difference across the sample. The stepwise procedure for taking the voltage readings is shown in Figure 4. It should be noted that once the current is supplied to the circuit, it will take time for the Peltier effect to cause significant changes in the measured electrical or thermal signals since the signals are measured at the sample holder whose large thermal mass requires more time to change the temperature difference than is allowed before noting the voltage difference. Steps 4 to 7 in Figure 4 were repeated till either of the following conditions were satisfied, i.e. the measured terminal voltage was zero (short circuit, I_{sc}, condition) or the electronic load reached its maximum current limit.

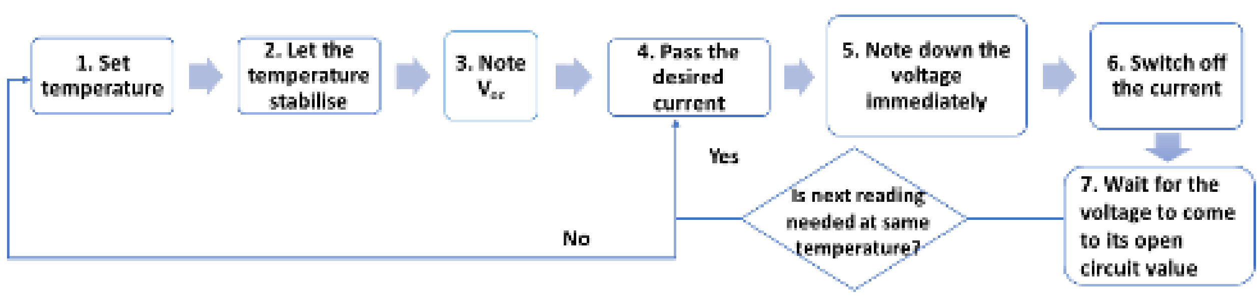

Figure 4 Procedure of obtaining CTD V-I plots at various set temperatures

Generally, for a given set temperature, when temperatures across the sample holder stabilize, the measured voltage has contribution from the sample and the Cu wires. The corrected sample voltage (V) is calculated as:

$$V = V_{measured} - V_{Cu} \tag{1}$$

V_{Cu} is the contribution from Cu wires given by,

$$V_{Cu} = -\int_{T_c}^{T_h} \alpha_{Cu}(T)dT \tag{2}$$

Data for the temperature dependent Seebeck coefficient of Cu were taken from literature[19]. The V-I curve is then plotted, as shown in Figure 5. For power output, the simple formula

$$P_{out} = V \times I \tag{3}$$

is used. A representative power parabola is also shown in Figure 5. The condition of maximum power is achieved when load resistance (R_{load}) equals the resistance of the sample (R_t), which is a sum of the sample resistance R_s and both contact resistances R_c towards the sample holder. The maximum power (P_{max}) is given by:

$$P_{max} = V_{oc}/2 \times I_{sc}/2 \tag{4}$$

I_{sc} is determined from the V-I curve either by direct measurement or from a linear approximation of the terminal voltage V, with R_t being the measured slope of the V-I curve.

$$V = V_{oc} - I \cdot R_t \rightarrow I_{sc} = \frac{V_{oc}}{R_t}\bigg| V \stackrel{\text{def}}{=} 0 \tag{5}$$

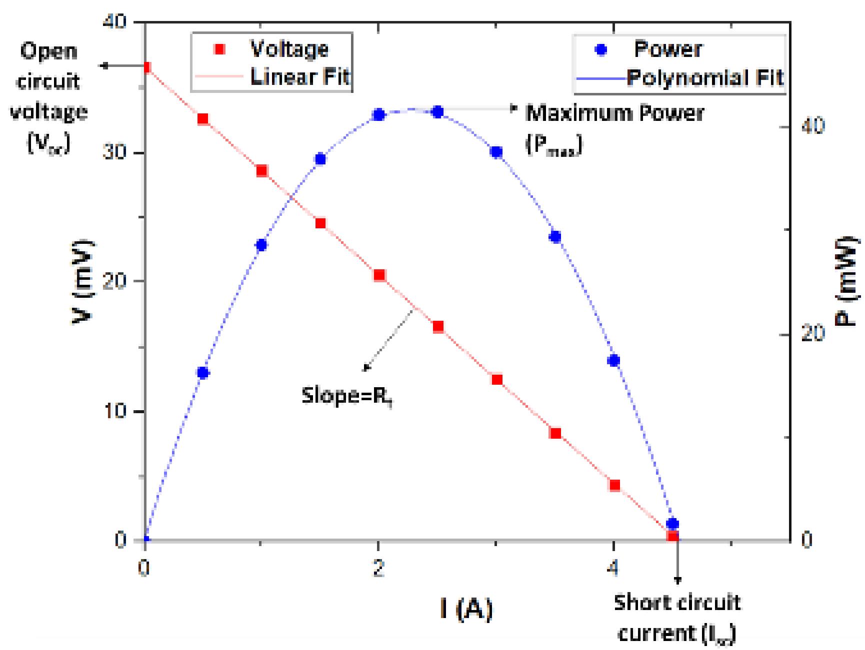

Figure 5 Representative P-I and V-I plot indicating the short circuit current, open circuit voltage, maximum power and total resistance measurement.

2. Efficiency and Radiation Correction

Fourier's law is used to calculate one-dimensional heat flow:

$$Q \quad = \kappa \quad \cdot A \cdot \nabla T \tag{6}$$

Here, κ is the thermal conductivity, A is the cross-sectional area of the material, and ∇T is the temperature gradient.

The heat flow through the reference SS 304 block in the open circuit condition, $Q_{oc,}$ is calculated using the reference block's thermal conductivity, κ_{ref}, its cross-sectional area, A_{ref}, and the temperature gradient across it, ∇T_{ref}. The data for thermal conductivity of SS 304 block are taken from literature[17]. κ_{ref} is taken at the mean temperature of the block $T_m{}'$, where $T_m{}' = \frac{T_4+T_6}{2}$. A transmission path for radiative crosstalk exists between the top and bottom parts of the sample holder which are not covered by the sample. This leads to an overestimation of heat flow through the sample. To calculate the contribution from the radiative heat bypass flowing through the lower reference block, Q_{rad}, everything except the heater, the bottom part of the sample holder, the lower reference block with its thermocouple and ceramic wool insulating the lower reference block, is removed for a radiation test. The heater is fixed with a mechanical support above the reference block with a gap similar to that in the normal run. The heat flow through the reference block is measured at different set temperatures (373 K, 473 K, 573 K, 673 K and 763 K) for the heater. The schematic of this setup is shown in Figure 6 (a). Temperatures are noted after stabilization, and the heat flow through the block is calculated using Equation 6. Thermal conductivity of SS 304 has been used. The cross-sectional area considered in the calculation is the difference between the cross-sectional area of the reference block and that of the TE leg (A_{sample}) since in leg measurements the cross section of the TE is not a part of the radiative transmission path, i.e.

$$Q_{rad} = \kappa_{ref} \cdot (A_{ref} - A_{sample}) \cdot \nabla T \qquad (7)$$

The top view of the reference block for the radiative test is shown in Figure 6 (b). Q_{rad} is then subtracted from transient and steady state heat flows measured in the normal run. A similar method has been employed by Hu *et al.* [11] in their high temperature gradient measurement setup.

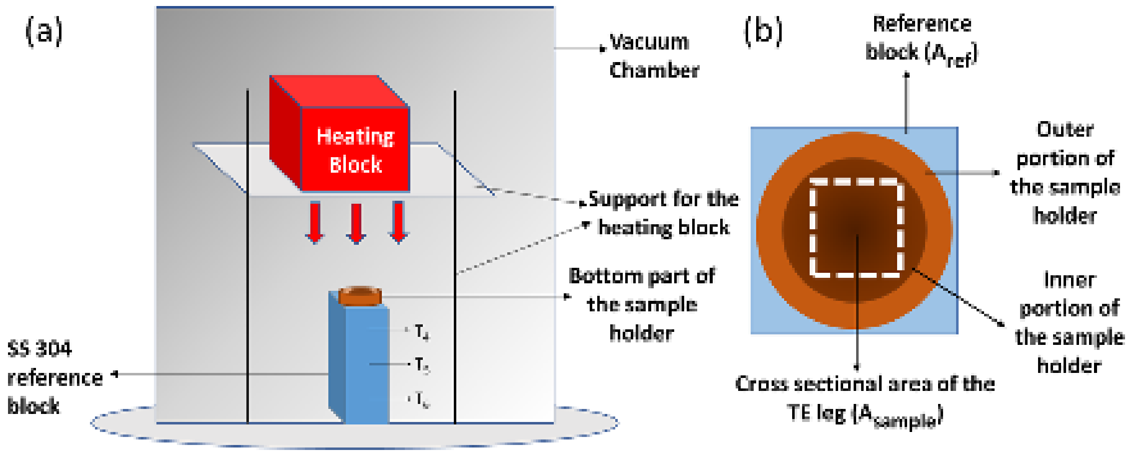

Figure 6 (a) Schematic of the setup for measuring the radiative contribution to the heat flow calculated from the cold side reference block (b) Top view of the reference block (not to scale). The dotted square indicates the cross-sectional area of the TE leg subtracted from the cross-sectional area of the reference block.

In the open circuit condition, assuming no radiative losses *from the sample* (practically no loss from the lateral surface of the sample through conduction and convection in vacuum), the heat flow through the hot side of the sample should equal the heat flow to its cold side. In presence of radiative heat losses of the sample the situation can potentially change, particularly if the sample is exposed to a high thermal gradient, since the sample will emit heat to the ambient along its side faces preferably at sections with higher temperatures, which will yield differences between the incident and outgoing heat of the sample. However, if the sample side areas are thermally insulated and insignificant in size compared to the area of the lower reference block outside the cross-sectional area of the sample (Fig. 6b), the dominant heat bypass by radiation is still given by the direct heat exchange between the heater and the lower sample holder/reference block. The calculation of a radiation-corrected incident heat flow into the sample from a measured heat flow at the cold side reference block Q_{oc} has therefore to account for this direct heat exchange by radiation, Q_{rad}. Under open loop conditions this yields an incident heat flow $Q_{oc} – Q_{rad}$. When current flows through the TE leg, Peltier heat is released at the junction of the leg and sample holder and causes changes in the incident heat flow, even in the short time for which the current is allowed to flow. The Joule heat which is very small in magnitude, however, does not alter the heat flow in this short time and is not included in the incident heat flow estimation under load. The CTD incident heat flow to the sample ($Q_{in,CTD}$) is given by:

$$Q_{in,CTD} = Q_{oc} - Q_{rad} + \alpha_H I T_H \quad (8)$$

Here, α_H is the Seebeck coefficient at hot side. Then the CTD efficiency (η_{CTD}) is:

$$\eta_{CTD} = P_{out}/Q_{in,CTD} \quad (9)$$

B. Continuous Current Flow (CCF) Measurements

To estimate the performance of a generator in working conditions, continuous current flow measurements have been performed.

When current is passed through a TE device, the Joule and Peltier heat components lead to variation in temperatures and sufficient time is needed for temperature stabilization before generating a *V-I* point. Also, V_{oc} (I_i) (instantaneous voltage after switching off the at the current *I*) has to be obtained to correct for the Peltier effect while calculating resistance from the continuous current *V-I* plot. The procedure for obtaining *V-I* plots is given in Figure 7. A set of *V-I* values are obtained till the short circuit current or the maximum current of the electronic load is reached.

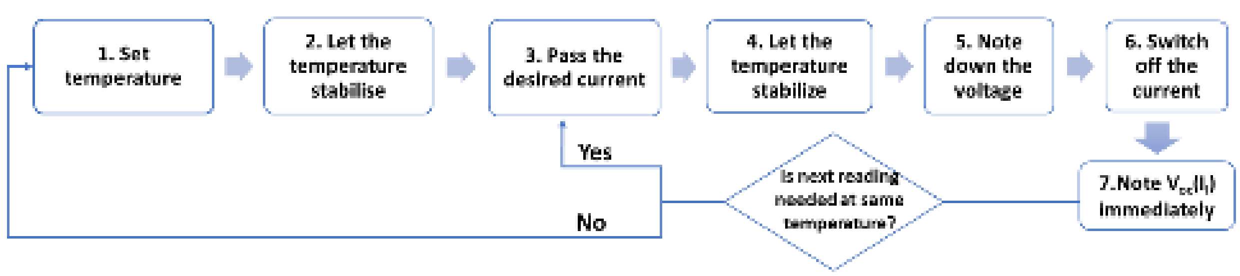

Figure 7 Procedure of obtaining steady state V-I plots at various set temperatures

After the temperatures stabilize, heat flow through the reference block under load, Q_{load}, is obtained using Equation 6. Also, due to localized heating at the screw joints (see metallic lugs in Figure 2(a)) on the cold side, half of the Joule heat liberated at the cold side sample holder, Q_{lh}, flows through the reference block. Just like Q_{rad}, this fraction (0.5* Q_{lh}) is not a part of the heat flowing through the sample. Therefore, it is also subtracted from Q_{load} to obtain the incident heat flow to the sample. Procedure to find Q_{lh} is given in Section IV. The same effect happens at the hot side but since here ("half of") the Joule heat, which is liberated at the contact between the sample and its holder, flows through the sample, it is already a part of Q_{load}. Heat input to the sample under CC condition, $Q_{in,CC}$, is given by:

$$Q_{in,CC} = Q_{load} - Q_{rad} + P_{out} - 0.5 * Q_{lh} \quad (10)$$

The efficiency is then calculated as:

$$\eta_{CC} = P_{out}/Q_{in,CC} \quad (11)$$

C. Material Properties

Material properties have been measured under high temperature differences during the CTD measurements. Seebeck coefficient and thermal conductivity are measured under open circuit conditions and electrical conductivity is measured using the *V-I* plots. Note that the material properties are measured as a function of the temperature difference (indicated by the subscript LTD standing for large temperature difference) and not a single temperature.

a. Seebeck Coefficient

After temperature stabilization and under open circuit conditions, the Seebeck coefficient of the sample is obtained using

$$\alpha_{LTD} = -V_{oc}/(T_h - T_c) \tag{12}$$

b. Electrical Conductivity

Slope obtained from *V-I* plots gives the total resistance being measured, i.e. R_t which is the sum of the contact resistance R_c and the sample resistance R_s. To calculate R_c, the room temperature *V-I* plot are generated. Room temperature resistance of the sample was calculated from the standard conductivity measurement of the material and the dimensions of the sample. Using this, the contact resistance is evaluated as

$$R_c = R_t - R_s. \tag{13}$$

The contact resistance is assumed to be independent of temperature and taken as a constant for subsequent measurements. Using this known value of R_c, electrical conductivity of the sample is obtained from CTD *V-I* plots generated under different temperature differences.

c. Thermal Conductivity

Under open circuit conditions, only conductive heat flow occurs (Equation 6). Thus, the heat flow through the cold side reference block will be equal to the heat flow into the sample at its hot side. However, Q_{rad} must be subtracted from Q_{oc} as Q_{rad} does not flow through the sample but is directly coupled into the cold side block by heat radiation from the surrounding. κ for the material was obtained using:

$$\kappa_{LTD} = (Q_{oc} - Q_{rad}) \times l/(\Delta T \times A_{sample}) \tag{14}$$

Here, $\Delta T = T_h - T_c$ and l is the length of the sample. It should be noted that κ_{LTD} includes contribution from the thermal resistance of the metallic sample holder parts and the thermal contact resistances between the sample, sample holder and the reference blocks, which are considered to be small compared to the large thermal resistance of TE-materials.

IV. RESULTS

A. Material Properties under Small Temperature Gradient

Small temperature difference α, σ, κ were measured on a pellet (synthesized from the same batch as the TE leg) between 300 K and 700 K. Subscripted SM has been used to denote standard measurements. α and σ were measured using a custom-built device while κ was measured using a laser flash apparatus. Thermal diffusivity (D) of the pellet was measured followed by the sequential measurement of electrical conductivity (σ) and Seebeck (α) coefficient in the same temperature cycle (300-700 K). The thermal conductivity of the pellet was calculated using the relation $\kappa = D \cdot C_p \cdot d$, d being the density of the sample (theoretical density of 2.97 g/cc was used)[20]. The specific heat capacity at constant pressure, C_p, for the composition was calculated from the Dulong-Petit limit for the specific heat capacity at constant volume, C_V^{DP}(0.534 J/g.K), using the relation: $C_p = C_V^{DP} + \frac{9E_t^2 T}{\beta_t d}$. Here, E_t is the linear coefficient of thermal expansion (1.68×10^{-5} K^{-1}) and β_t is the isothermal compressibility (2.19×10^{-11} Pa^{-1})[20]. The temperature variation of α, σ, κ and zT from standard measurements is shown in Figure 8. Polynomial fits were obtained for these data sets. The obtained coefficients for the polynomial equation ($a + b\cdot T + c\cdot T^2 + d\cdot T^3$) are given below:

For $\alpha(T)$ *in* $\mu V/K$: a = 64.14918, b = -1.0597, c = 0.00133, d = -6.2726x10^{-7}

For $\sigma(T)$ *in S/cm:* a = 3192.64898, b = -9.54088, c = 0.01302, d = -6.73732x10^{-6}

For $\kappa(T)$ *in W/mK*: a = -0.10676, b = 0.01745, c = -4.04769 x10^{-5}, d = 2.86927 x10^{-8}

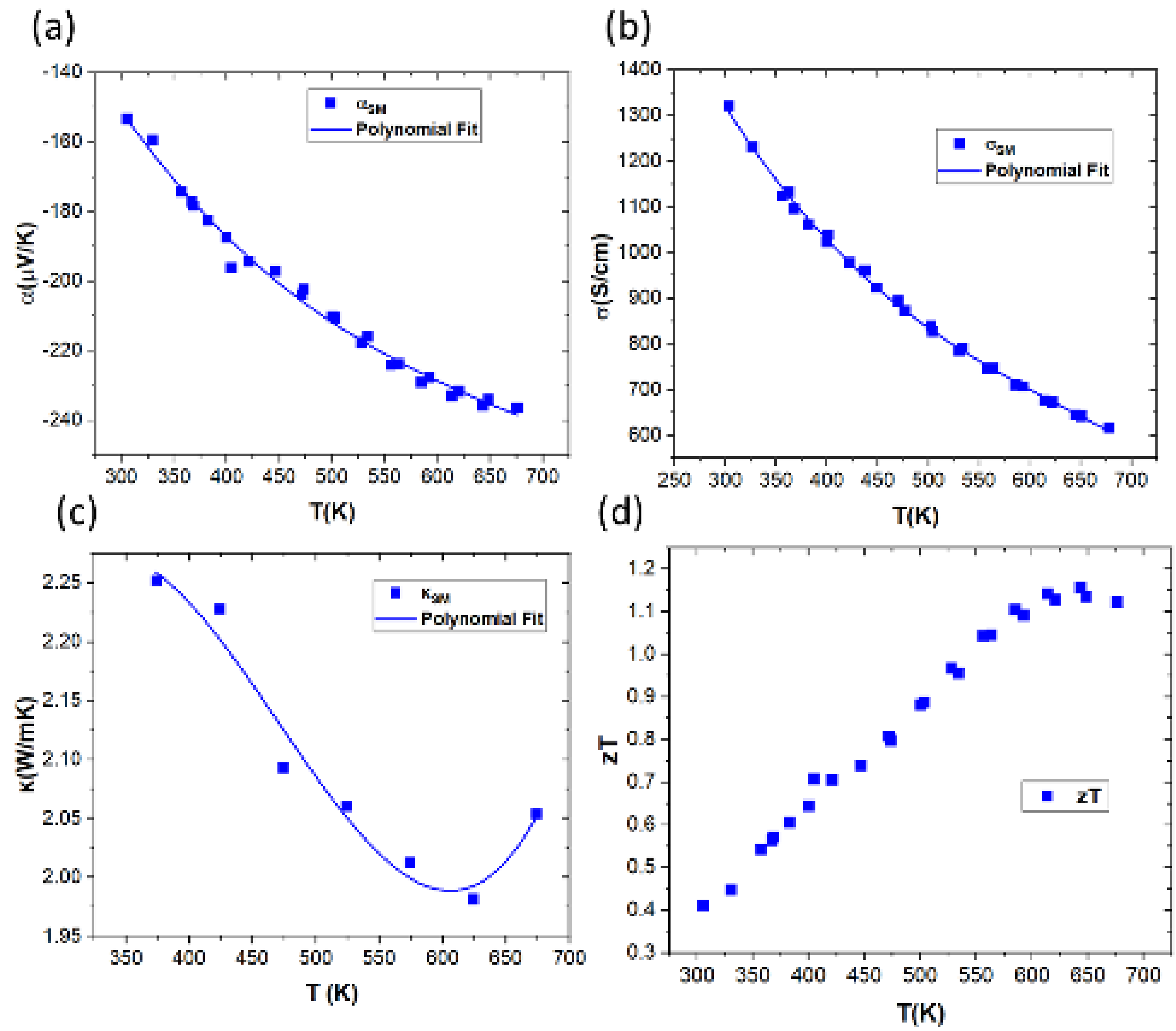

Figure 8 Seebeck coefficient (a), electric conductivity (b) and thermal conductivity (c) from standard measurements under small temperature gradient obtained on an $Mg_{2.2}(Si_{0.3}Sn_{0.7})_{0.9927}Bi_{0.0073}$ pellet. zT (d) is obtained indirectly from α, σ and κ.

B. Material Properties under Large Temperature Differences

Material properties measured under large temperature differences are plotted in Figure 9 along with reference values. Polynomial fits of TE properties for the data obtained from standard measurements were used to calculate the reference values. Averaging formulae for calculating material and device properties with the hot and cold side temperatures, T_h and T_c, respectively, for a given TE property, $M(T)$, are listed below[21, 22].

(i) Area under the curve (M_{av}):

$$M_{av} = \frac{1}{\Delta T}\int_{T_c}^{T_h} M(T)dT \tag{15}$$

(ii) Value at mean temperature (M_{tm}):

$$M_{tm} = M(T_m) \tag{16}$$

Here, $T_m = \frac{T_h+T_c}{2}$

(iii) Mean value (M_m):

$$M_m = \frac{M(T_h)+M(T_c)}{2} \tag{17}$$

(iv) Logarithmic average (M_L):

$$M_L = \frac{1}{\ln\left(\frac{T_h}{T_c}\right)}\int_{T_c}^{T_h} \frac{M(T)}{T} dT \tag{18}$$

It should be noted that the electrical and thermal conductivity averages using Equations 15 and 18 were obtained by first taking the polynomial fits for their corresponding resistivities because physically, the integrals are sums over infinitesimal sections of the TE leg in series, and resistive elements are summed in series while conductive elements are summed in parallel. Error bars for α_{LTD}, σ_{LTD} and κ_{LTD} are 5%, 3% and 5% respectively. For the Seebeck coefficient, all calculated values are within the error bars. For electrical conductivity, at larger temperature gradients, the experimental results show good agreement with calculated values using temperature mean and integral averaging. However, the errors are higher for thermal conductivity which is partly due to the difficulty associated with heat flow measurement. Also, a recent study has shown that area under the curve averaging (Equation 15) is the most accurate among the four averaging formulae listed here[3] to estimate the Seebeck coefficient. This validates the measurement setup for the measurement of Seebeck coefficient. In the same study, it has been suggested that pure temperature averaging of electrical and thermal conductivities are bound to be inaccurate, and spatial averaging is needed. Thus, discrepancies between the experimental LTD properties and the temperature averaged properties are not necessarily or entirely linked with instrument accuracy. The temperature-averaged and experimental zT values shown in Figure 9(d) are obtained using $zT = (\alpha^2 \cdot \sigma / \kappa) \cdot T_m$ where averaged and experimental individual TE properties, respectively, are taken.

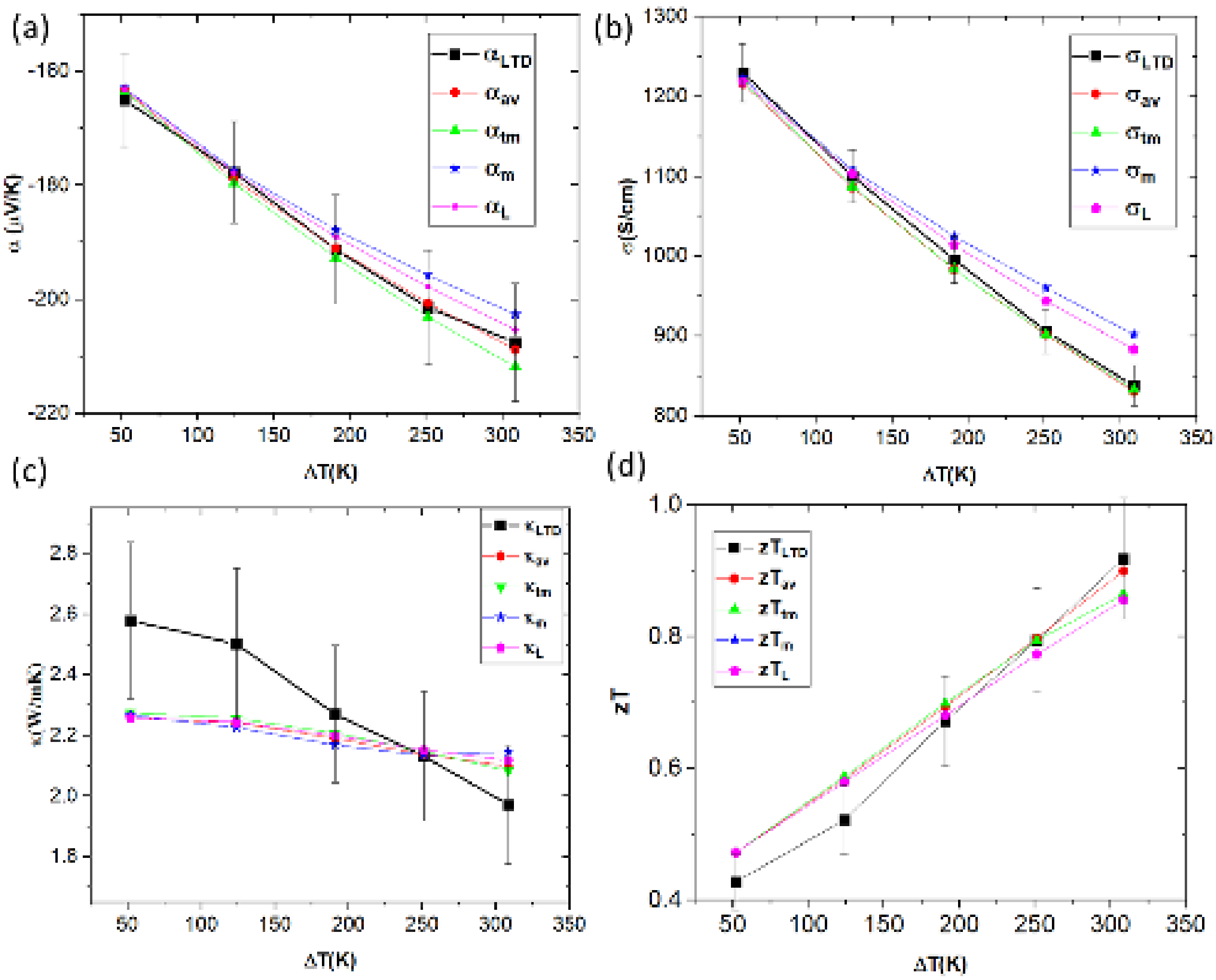

Figure 9 (a) Seebeck coefficient (b) Electrical Conductivity (c) Thermal conductivity obtained from large temperature difference measurements (black) and different averaging methods. The error bars are 5%, 3% and 10%, respectively. (d) zT obtained indirectly from α, σ and κ with a 10% error bar.

C. Power Output and Efficiency from CTD measurements

Figure 10 shows the room temperature plot used to obtain the contact resistance. Based on the obtained value of R_c = 17 μΩ cm^2 the soldering of the metallized TE leg to the sample holder using Zn was successful.

It was observed that the temperature-averaged TE properties did not differ among each other, i.e., they were all within the error bars for α and κ and σ_{av} and σ_{Tm} were within the error bars for σ. Since area under the curve averaging has been reported to be more accurate than other methods and is also within the error bars for all TE properties, it is the only one which has been used for calculating the reference *V-I* and *P-I* plots for simplicity. Reference voltage and theoretical power as a function of current, $V_{ref}(I)$ and $P_{out,ref}(I)$ are obtained using the following formulae

$$V_{ref}(I) = -\alpha_{av} \cdot \Delta T - (R_{av} + R_c) \times I \quad (19)$$

$$P^{CTD}_{out,ref}(I) = V_{ref}(I) \times I \quad (20)$$

Here, R_{av} is obtained from σ_{av} and leg dimensions. Experimental and reference *V-I* and *P-I* curves are shown in Figure 11. Various parameters obtained experimentally are listed in Table I.

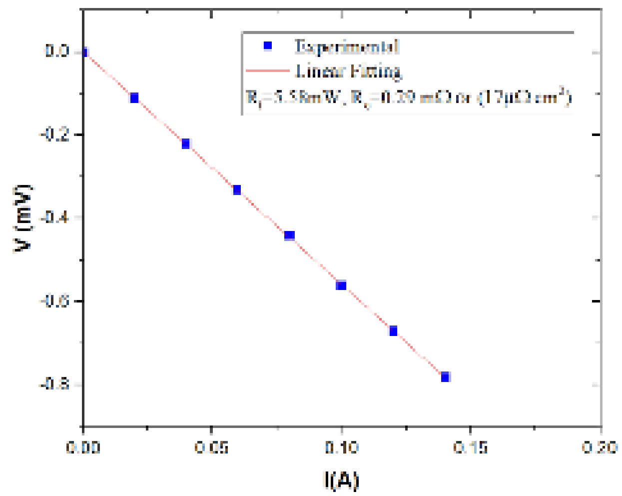

Figure 10 Room temperature measurement on the TE leg used to find the contact resistance R_c

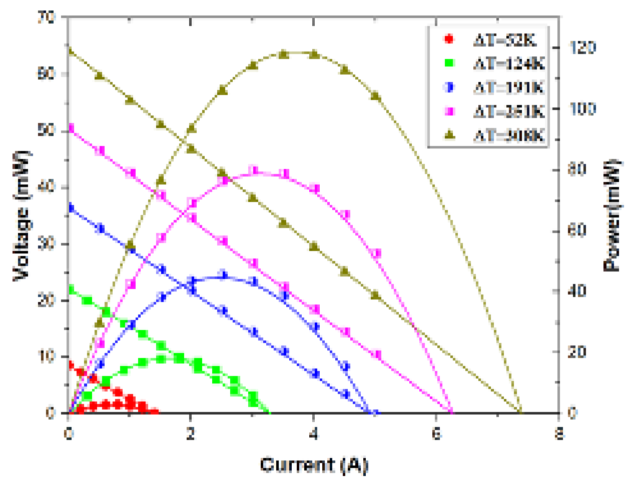

Figure 11 Experimental and reference P-I and V-I plots. Symbols represent experimental data while the solid curves represent the corresponding theoretical curves.

Table I: Measured properties of the TE leg with varying temperature difference

T_h (K)	ΔT (K)	α_{LTD} (μV/K)	σ_{LTD} (S/cm)	κ_{LTD} (W/mK)	V_{oc} (mV)	I_{sc} (A)	R_s (mΩ)	P_{max} (mW)	η_{max} (%)
356.44	52.07	-164.97	1229.46	2.58	8.59	1.43	5.69	3.1	1.32
438	123.84	-177.73	1100.48	2.50	22.01	3.31	6.36	18.2	3.16

514.99	190.71	-191.23	995.92	2.27	36.47	4.98	7.03	45.4	5.21
586.16	251.13	-201.45	905.94	2.13	50.59	6.31	7.73	79.9	6.98
655.55	308.5	-207.55	837.98	1.97	64.03	7.40	8.35	118.5	8.59

For obtaining theoretical efficiencies, the formulae used are

(i) Constant property formula[21] with contact resistance, where $\delta = \frac{R_c}{R_s}$ and R_s=R_{av}.

$$\eta_{max} = \frac{(T_H - T_C)}{T_H} \frac{\left((1+\delta)^2 + (1+\delta)ZT_M\right)^{\frac{1}{2}} - (1+\delta)}{\left((1+\delta)^2 + (1+\delta)ZT_M\right)^{\frac{1}{2}} + \frac{T_C}{T_H}(1+\delta)} \tag{21}$$

Using Equations 15-18, different $Z\ (= \alpha^2\sigma/\kappa)$ values were calculated to obtain maximum efficiencies η_{av}, η_{tm}, η_m and η_L.

(ii) Efficiency from engineering figure of merit[22]

$$\eta_{eng} = \eta_c \frac{\sqrt{1+(ZT)_{eng}\left(\acute{\alpha}/\eta_c - 1/2\right)} - 1}{\acute{\alpha}\left(\sqrt{1+(ZT)_{eng}\left(\acute{\alpha}/\eta_c - 1/2\right)} + 1\right) - \eta_c} \tag{22}$$

(iii) Efficiency from engineering figure of merit including the contact resistance[23],

$$\eta_{engc} = \frac{\sqrt{1+\frac{(ZT)eng}{\delta+1}\left(\frac{\acute{\alpha}}{\eta_C} + \frac{2\ \delta-1}{2(\ \delta+1)}\right)} - 1}{\acute{\alpha}\ \left(\sqrt{1+\frac{(ZT)eng}{\delta+1}\left(\frac{\acute{\alpha}}{\eta_C} + \frac{2\ \delta-1}{2(\ \delta+1)}\right)} + 1\right) - 2\eta_C \frac{2\ \delta-1}{2(\ \delta+1)}} \tag{23}$$

Equations 22 and 23 use, $(ZT)_{eng} = \frac{\left(\int_{T_C}^{T_h} S(T)dT\right)^2}{\int_{T_C}^{T_h} \rho(T)dT \int_{T_C}^{T_h} \kappa(T)dT}\Delta T$ and $\acute{\alpha} = \frac{S(T_H)\Delta T}{\int_{T_C}^{T_h} S(T)dT}$

Maximum experimental efficiency (η_{exp}) was calculated as a function of current, $\eta_{max}(I)$ as

$$\eta_{max}(I) = max\left(\frac{(V_{oc} - IR_t)I}{Q_{oc} - Q_{rad} + S_H I T_H}\right) \tag{24}$$

Efficiencies as a function of temperature difference calculated using the different equations along with the experimental data are plotted in Figure 12 (a). The match between experimental and calculated efficiencies is not as good at smaller temperature differences due to the relatively poor estimation of thermal conductivity at lower temperature differences. However, all calculated efficiencies lie within 10% of the maximum experimental efficiency at high temperature differences. Thus, a single best formula for determining efficiency cannot be concluded upon.

Calculation of the reference maximum power output was carried out using

$$P^{ref}_{max,CTD} = \frac{(\alpha \cdot \Delta T)^2}{4(R_s + R_c)} \tag{25}$$

Using different temperature-averaged values for α and σ (for R_s) (Equations 15-18), various averaged reference values were calculated. Comparison of experimental and theoretical maximum power output is shown in Figure 12 (b). There is an excellent match between the experimental and theoretical maximum powers over the entire temperature range.

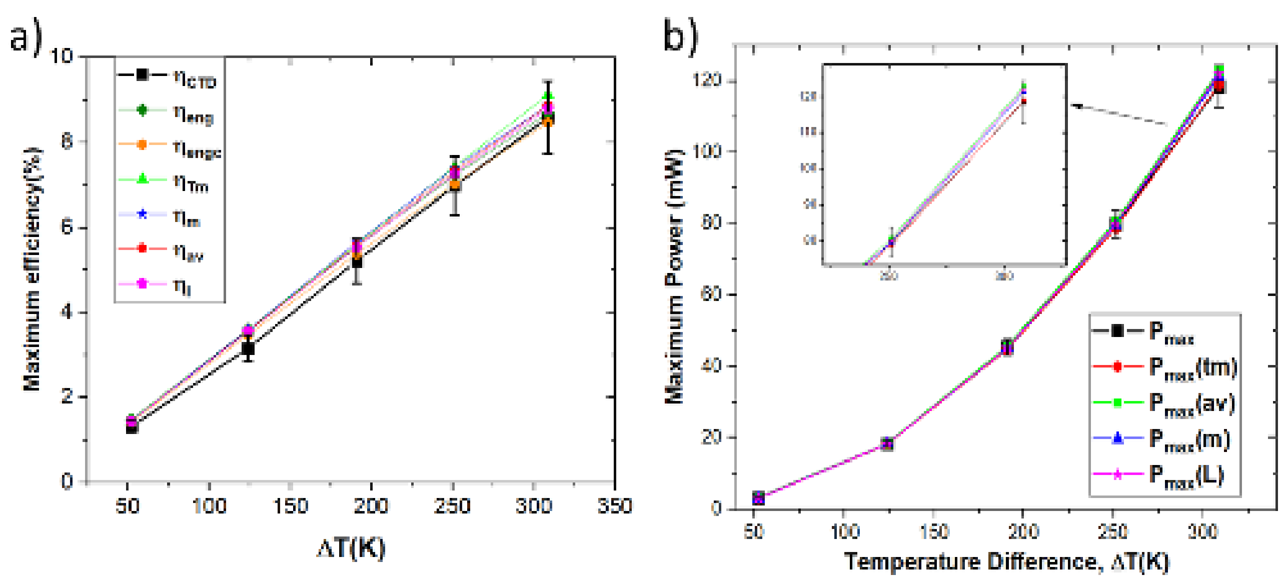

Figure 12 Comparison of experimentally determined (a) maximum efficiency and (b) maximum power with theoretical results obtained from different averaging methods.

TABLE II: Comparison between experimentally determined maximum efficiency (%) and theoretical values obtained from different averaging methods.

$\Delta T(K)$	η_{exp}	η_{tm}	η_{av}	η_{eng}	η_{engc}	η_{m}	η_{L}
52	1.32	1.45	1.45	1.49	1.43	1.45	1.45
123	3.16	3.58	3.57	3.60	3.48	3.59	3.55
190	5.21	5.61	5.57	5.55	5.38	5.64	5.53
251	6.98	7.44	7.33	7.23	7.03	7.41	7.27
308	8.59	9.11	8.86	8.69	8.47	8.86	8.80

D. Continuous Current Flow (CCF) Measurements

Steady-state measurements were done for two set temperatures - 373 K and 763 K of the heater controller. When current flows through a material, due to current dependent effects- Peltier effect, Ohmic Heating and Thomson effect, temperature difference across it changes. In CCF measurements, different constant current values have been set and passed through the TE leg till the temperature difference stabilized at each current setpoint. For calculations of the CCF heat flow Thomson's coefficient (τ) was included and the formulae used for obtaining reference power output and efficiency are[24]:

$$P^{ref}_{out,CCF}(I) = \Big((\alpha_H T_{H-}\alpha_c T_c) - \big(R_{S,Tm} + R_c\big)I\Big) \times I - \tau_{Tm} I \Delta T \tag{26}$$

$$Q^{ref}_{out,CCF}(I) = \alpha_c I T_c + \kappa_{Tm}\Delta T + 0.5\big(R_{S,Tm} + R_c\big)I^2 + 0.5\tau_{Tm} I \Delta T \tag{27}$$

Both reference power and efficiency were calculated at each current value as in the experiment. Figures 13 and 14 show the measurements under steady state for open circuit temperature differences of 52 K and 308 K respectively. The cold side temperature is expected to increase due to contributions from Peltier heat transport and Ohmic heating. On the hot side however, Peltier heat is being absorbed and Ohmic heat is being released. Additionally, because current flows through the circuit in the CCF measurements for much longer than in the transient measurements, a high contact resistance between the Cu lugs and connecting wires would lead to the liberation of a substantial amount of Joule heat. This Joule heating (called screw heating in Section III (B)), on the hot side, could possibly counteract the Peltier effect on the hot side even leading to increased temperature on the hot side and on the cold side, it would increase the temperature alongside the Peltier effect. This hypothesis could explain the temperature profiles in Figures 13 (a) and 14 (a) as a function of current. Overall, the temperature difference decreases with current (Figures 13(b) and 14 (b)). On the cold side, this additional screw heating is being calculated as a part of Q_{out} even though it is not a part of heat flowing though the sample. This additional localized heating due to contact resistance due to the connectors, Q_{lc} was calculated using

$$Q_{lc} = Q_{load}(I) - Q_{rad} - Q_{out,CCF}^{ref}(I) \tag{28}$$

The resistance was calculated for each data point using $R_{screw} = Q_{lc}/I^2$and an average resistance ($\bar{R}_{screw}$) was taken. This average resistance was then used to deduct the additional heat from the measured heat using

$$\bar{Q}_{lc} = I^2 \bar{R}_{screw} \tag{29}$$

$\bar{R}_{screw}$ value at $\Delta T_{oc} = 52$ K is 126 mΩ and at $\Delta T_{oc} = 308$K is 29 mΩ, with standard deviations of 52 mΩ and 23 mΩ, respectively. The high standard deviation is most likely due to the uncertainty in radiation correction. This correction does not appear in CTD efficiency measurement because the current flows through the circuit for relatively much less time, which prevents significant heating at the screws.

The impact of reducing temperature differences on the *V-I* characteristics is evident from Figures 13(c) and 14 (c), which show declining open circuit voltage with increasing current. To obtain the corrected resistance from these plots, the following equation is used[25]:

$$R_t = \frac{\Delta V_1 - \Delta V_2}{I_1 - I_2} \tag{30}$$

Here $\Delta V_i = V_{oc}(I_i) - V(I_i)$. The total resistances are obtained using Equation 27 and is found to be 6.07 mΩ and 10.40 mΩ for $\Delta T_{oc} = 52$ K and 308 K respectively. CTD measurement slopes for similar temperature differences are 5.98 mΩ and 8.64 mΩ. Experimental power output and efficiency have been compared with their reference values and the results are shown in Figures 13 (d) and 14 (d).

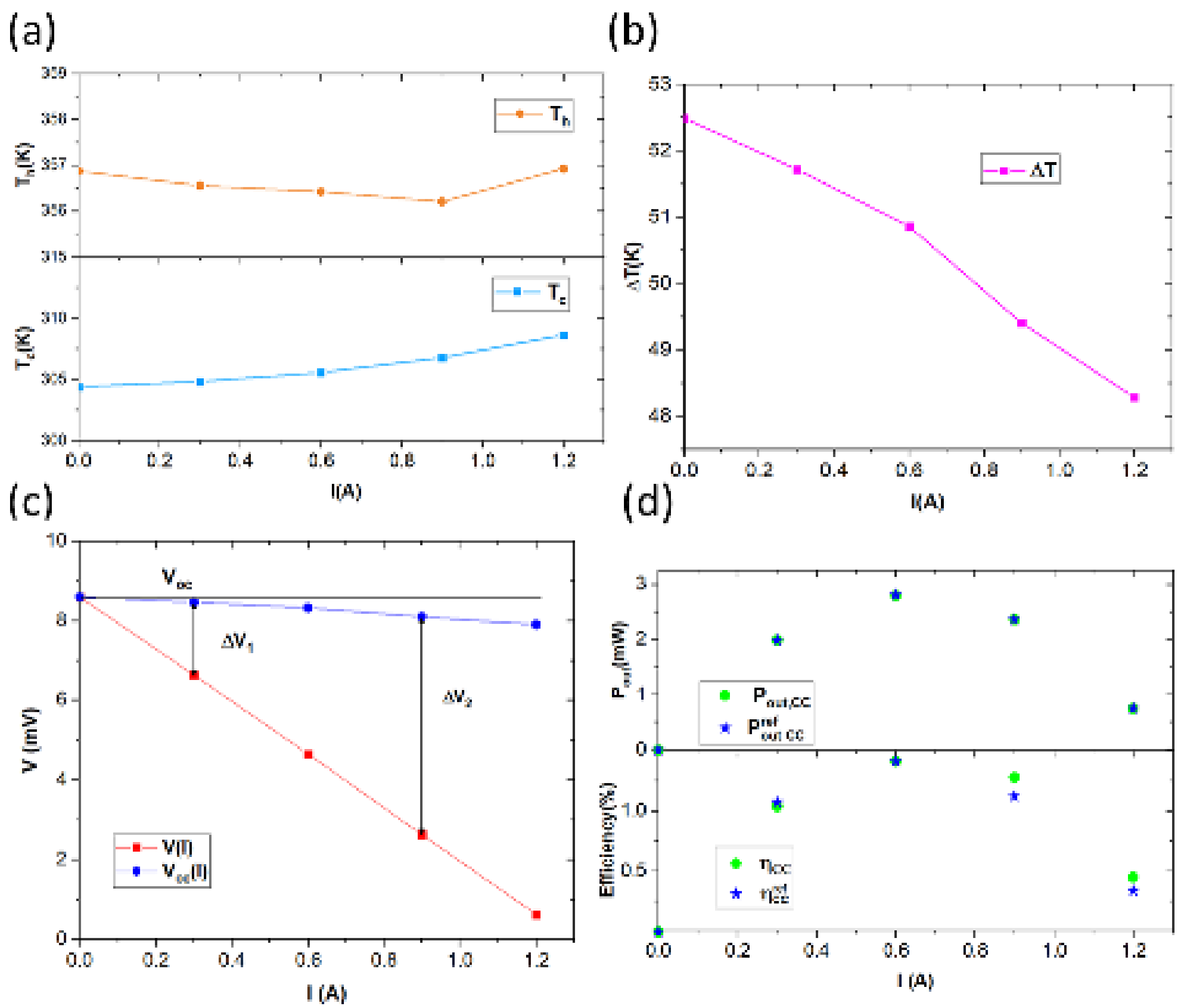

Figure 13 Experimental data from the continuous current flow measurements at open circuit temperature difference of 52 K. (a) Hot side (T_h) and cold side (T_c) temperature and (b) temperature difference as functions of current. (c) V- I curve obtained during steady state measurement (d) Reference and experimental power output and efficiency as functions of current.

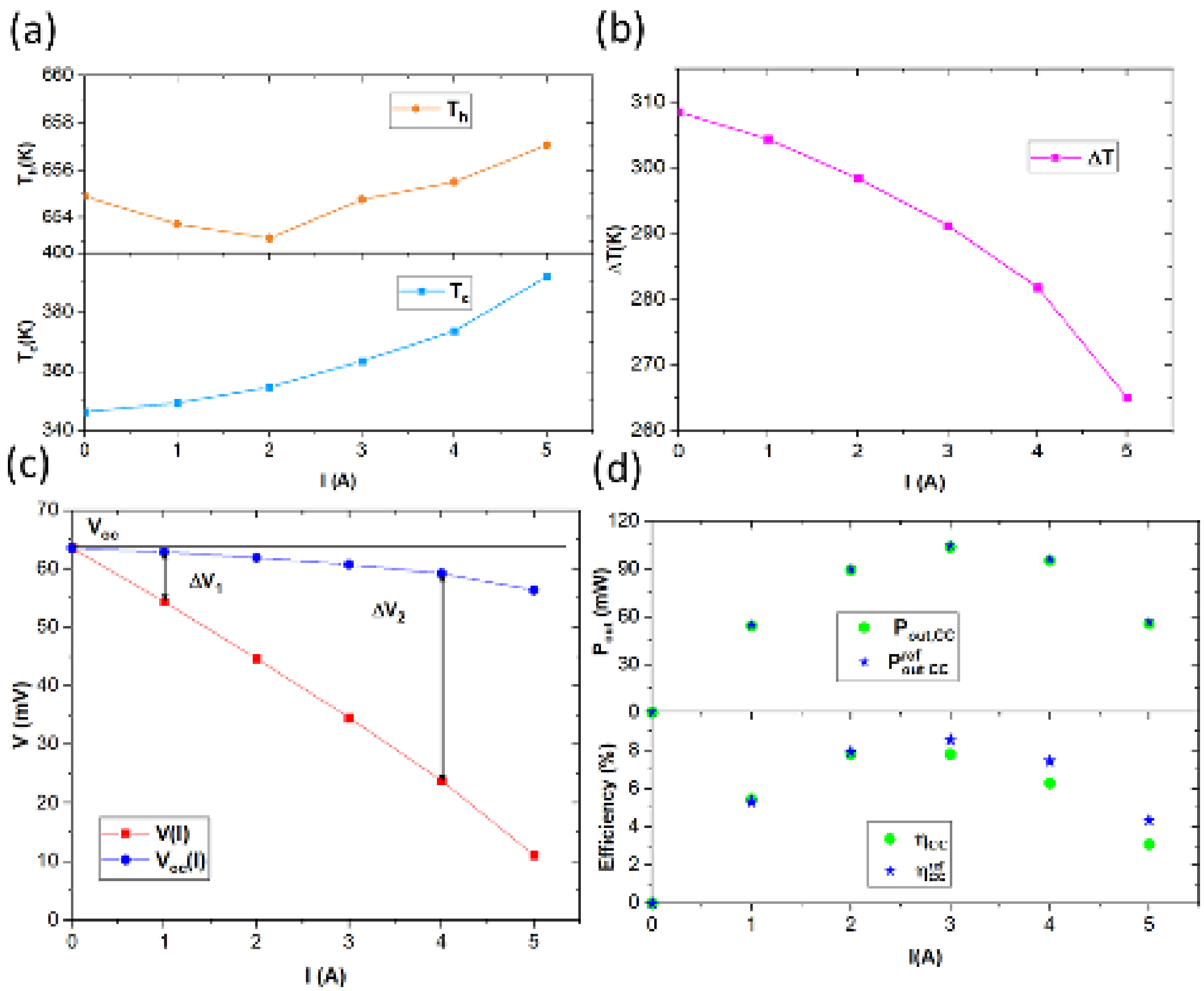

Figure 14 Experimental data from continuous current flow measurements at open circuit temperature difference of 308 K. (a) Hot side (T_h) and cold side (T_c) temperature and (b) temperature difference as functions of current. (c) V-I curve obtained during steady state measurement (d) Reference and experimental power output and efficiency as functions of current.

V. DISCUSSION

A. Comparison between CTD and CCF Power and Efficiency

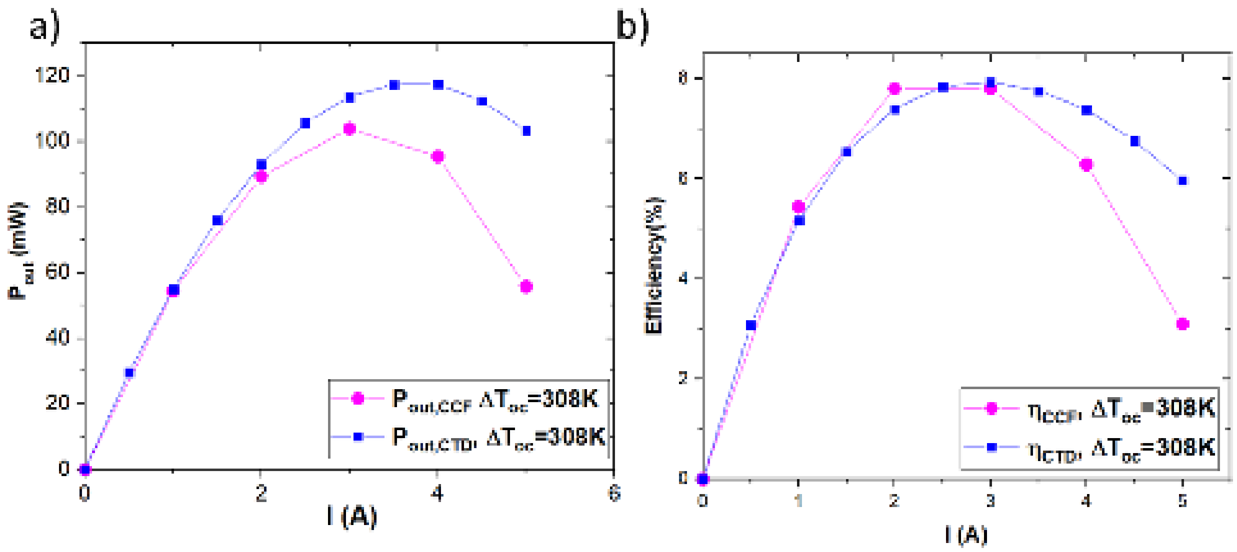

Figure 15 (a) Comparison of (a) power output and (b) efficiency from continuous current and constant temperature difference measurements at an open circuit temperature difference of 308 K.

A comparison of the CCF and CTD power (Figure 15 (a)) shows that starting from the same open circuit temperature difference, the power output under continuous current flow keeps on decreasing with increasing current when compared to the CTD power output with same current. This is the effect of the decreasing temperature difference with increasing current shown in Figures 14 (b). The decreasing temperature difference causes a lowering of the open circuit voltage, which effectively pretends an increase in the electric resistance. Thus, the total resistance obtained for the CCF and CTD measurements are 10.39 mΩ and 8.59 mΩ, respectively. The higher resistance of the circuit in CCF measurements lowers the measured maximum power output according to Equation 25. Moreover, the current corresponding to maximum power output in the CTD condition is ~20% higher than that of the CCF measurement. Therefore, while theoretically estimating the performance of a CCF operation (reflecting application conditions), especially with respect to the current or load for maximum power output or maximum efficiency, it is necessary to include the effect of current based phenomenon on the temperature difference as this reduces the generated thermopower leading to decrease in power output, similar to a real application scenario, which will be exposed to finite thermal conductivities along the heat transmission paths, too.

Figure 15 (b) shows a comparison of CTD and CCF efficiency at ΔT=308 K. The CCF efficiencies are lower than their CTD counterparts, especially at higher current values. This can be attributed to decreasing temperature difference as a function of the current in CCF measurements. It must however be highlighted that the decrease in ΔT is a consequence of increase in T_c to which screw heating gives a significant contribution. This problem is not expected to occur if modules with multiple legs are tested because the increased heat flow, which makes any heating at connection points of signal and supplying leads negligible if corresponding contact resistances can be kept low. For greater clarity, comparison of the relative difference in the CTD and CCF power outputs and efficiencies, given by $\frac{M_{CTD}-M_{CCF}}{M_{CCF}} * 100\%$, where M denotes the quantity of interest, at corresponding CCF current values is shown in Figure 16.

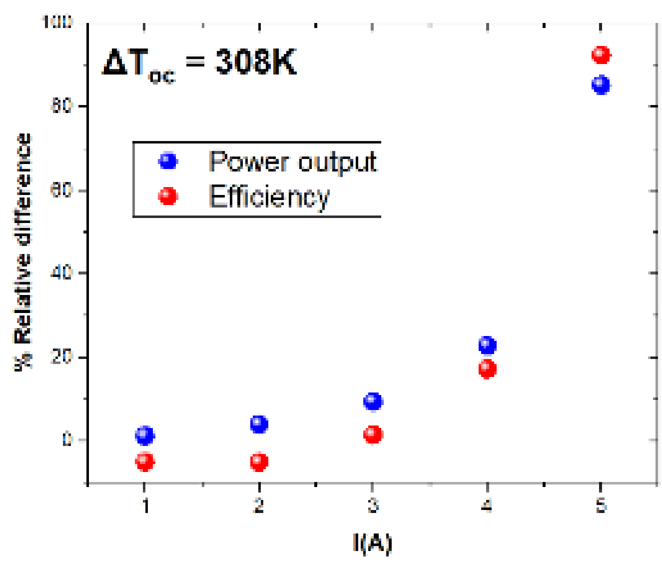

Figure 16 Relative difference in the CTD measurements of power output and efficiency with respect to the CCF measurements as a function of current for ΔT_{oc} = 308K

B. Error Analysis (CTD Measurement)

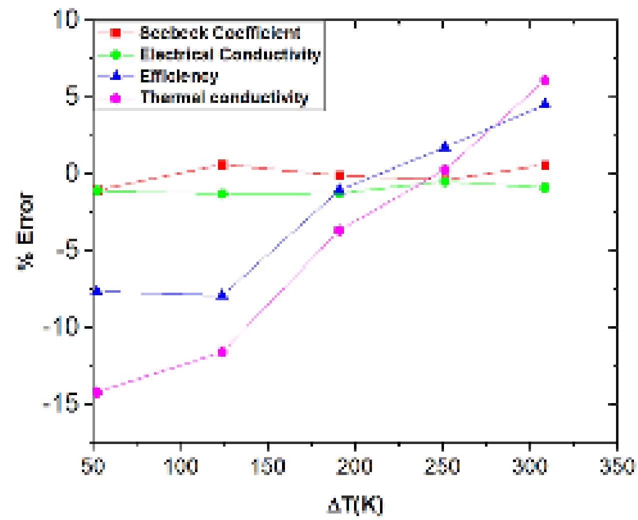

Figure 17 Relative error in Seebeck coefficient, Electrical conductivity, Thermal conductivity and Efficiency obtained from CTD measurements.

Relative error vs. temperature difference for Seebeck coefficient, thermal conductivity, electrical conductivity and efficiency based on CTD measurements are shown in Figure 17. Relative error was calculated using $\frac{M_{exp}-M_{ref}}{M_{ref}}$. Reference values are obtained from the area under the curve formulae (Equation 15) for α, σ and κ. Efficiency error comparison has been shown with the reference efficiency taken as η_{engc} (Equation 23). As seen in Figure 17, the errors in the Seebeck coefficient and electrical conductivity are relatively small (less than 2%). There are various reasons for this. First of all, it must be mentioned that since the comparisons are based on the averaging methods employed on experimental data from standard TE properties-measurements, which inherently have some error (standard error of 5% and 4% for α and σ, respectively [26] and 5% for kappa), the relative error does not actually compare with true values. An additional advantage of a high temperature gradient Seebeck measurement is that the relative uncertainty in the measured temperature difference becomes smaller as the difference increases. Also, a good contact between the sample and the holder lowers the errors. Using spatial averaging along with temperature averaging, further reduction in error is perhaps possible[3] for electrical and thermal conductivities and can be attempted.

VI. CONCLUSION

Experiments were accomplished up to a temperature difference of ~300 K with a maximum hot side temperature of ~673 K. The presented setup is reliable for power output and efficiency measurements and also for determination of various thermoelectric properties (Seebeck coefficient, electrical conductivity, and thermal conductivity) under large temperature gradients. Good electric contact (17 $\mu\Omega$ cm^2) was established between the tested material and the sample holder, which could be proven by the match between the experimental and calculated TE properties using various averaging techniques (within 3%,5% and 10% error bars for α, σ and κ, respectively). The contacting, however, is material specific. The setup can be used to analyze the performance of a material under working conditions, i.e. when current flows continuously through the material under which the temperature difference across the material can be significantly different from the one in open circuit condition. It was shown that the current corresponding to maximum power output can differ significantly when the temperature difference is maintained constant (20% higher) compared to a more practical scenario where temperature difference reduce under electric current flow due to the impact of the Peltier effect. With the help of this apparatus, it is not only possible to measure thermoelectric properties of a single leg under high temperature gradient but also to optimize contacting technologies. Measurements under continuous current flow conditions can also guide us in the optimization of materials suitable for practical applications.

ACKNOWLEDGMENTS

Financial support is gratefully acknowledged for the project “Thermoelectric Standardization for High Temperatures” (TEST-HT, grant number 03VP04401), which was granted by the German

Federal Ministry of Education and Research. TD acknowledges financial support provided by IRCC IIT Bombay (Grant No. RI/0317-10001389-001).

REFERENCES

[1]D. Champier, Energy Conversion and Management 140,167 (2017).
[2]T. Tritt and D. Rowe, (CRC Press Boca Raton, FL:, 2005).
[3]P. Ponnusamy, J. de Boor and E. J. A. E. Müller, Applied Energy 262,114587 (2020).
[4]B. Ryu, J. Chung and S. J. I. Park, Iscience 24,102934 (2021).
[5]C. Goupil, *Continuum theory and modeling of thermoelectric elements* (John Wiley & Sons, 2015).
[6]J. Corcoran, S. Raja and P. B. Nagy, NDT & E International 94,92 (2018).
[7]K. A. Borup, J. De Boor, H. Wang, F. Drymiotis, F. Gascoin, X. Shi, L. Chen, M. I. Fedorov, E. Müller and B. B. Iversen, Energy & Environmental Science 8,423 (2015).
[8]F. Edler and K. Huang, Measurement Science and Technology 32,035014 (2020).
[9]J. Martin, Measurement Science and Technology 24,085601 (2013).
[10]J. Martin, Review of Scientific Instruments 83,065101 (2012).
[11]X. Hu, A. Yamamoto, M. Ohta and H. Nishiate, Review of Scientific Instruments 86,045103 (2015).
[12]A. Muto, D. Kraemer, Q. Hao, Z. F. Ren and G. Chen, 80 (2009).
[13]Q. Zhu and Z. Ren, Energy 191,116599 (2020).
[14]G. K. Goyal, S. Mukherjee, R. C. Mallik, S. Vitta, I. Samajdar and T. Dasgupta, ACS Appl. Energ. Mater. 2,2129 (2019).
[15]W. Liu, X. Tang and J. J. J. o. P. D. A. P. Sharp, Journal of Physics D: Applied Physics 43,085406 (2010).
[16]X. J. Tan, W. Liu, H. J. Liu, J. Shi, X. F. Tang and C. Uher, Physical Review B 85,205212 (2012).
[17]R. S. Graves, T. G. Kollie, D. L. McElroy and K. E. Gilchrist, International Journal of Thermophysics 12,409 (1991).
[18]G. K. Goyal and T. Dasgupta, ACS Applied Materials & Interfaces 13,20754 (2021).
[19]N. Cusack and P. Kendall, Proceedings of the Physical Society 72,898 (1958).
[20]H. Kamila, P. Sahu, A. Sankhla, M. Yasseri, H.-N. Pham, T. Dasgupta, E. Mueller and J. de Boor, Journal of Materials Chemistry A 7,1045 (2019).
[21]A. F. Ioffe, *Semiconductor thermoelements and thermoelectric cooling* (Infosearch, Ltd., London, England, 1957).
[22]H. S. Kim, W. Liu, G. Chen, C.-W. Chu and Z. Ren, Proceedings of the National Academy of Sciences 112,8205 (2015).
[23]C. L. Hapenciuc, T. Borca-Tasciuc and I. N. Mihailescu, 7,045007 (2017).
[24]G. Fraisse, J. Ramousse, D. Sgorlon and C. Goupil, Energy Conversion and Management 65,351 (2013).
[25]P. Ziolkowski, P. Blaschkewitz and E. Müller, Measurement 167,108273 (2021).
[26]P. Ziolkowski, C. Stiewe, J. de Boor, I. Druschke, K. Zabrocki, F. Edler, S. Haupt, J. König and E. Mueller, Journal of Electronic Materials 46,51 (2017).

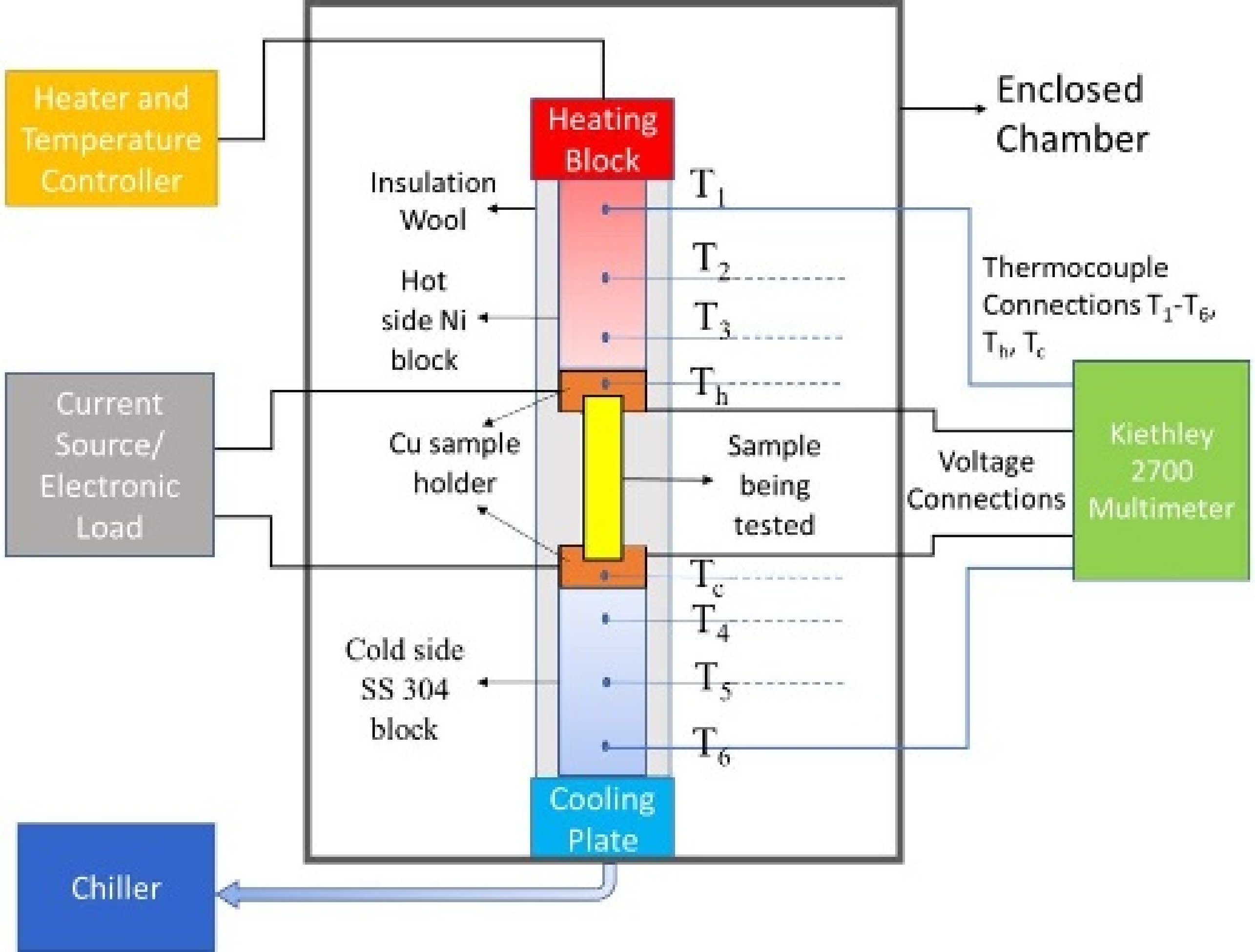
Heater and Temperature Controller
Heating Block
Enclosed Chamber
Insulation Wool
T_1
T_2
Hot side Ni block
T_3
Thermocouple Connections T_1-T_6, T_h, T_c
Current Source/ Electronic Load
T_h
Cu sample holder
Sample being tested
Voltage Connections
Kiethley 2700 Multimeter
T_c
T_4
Cold side SS 304 block
T_5
T_6
Cooling Plate
Chiller

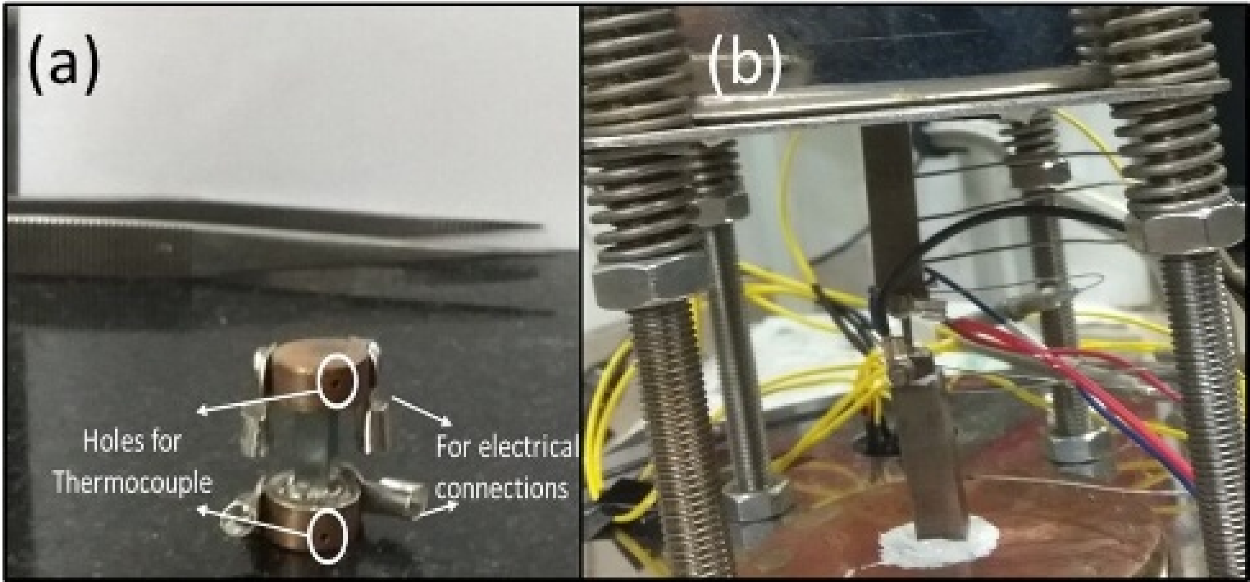
(a)
Holes for
Thermocouple
For electrical
connections
(b)

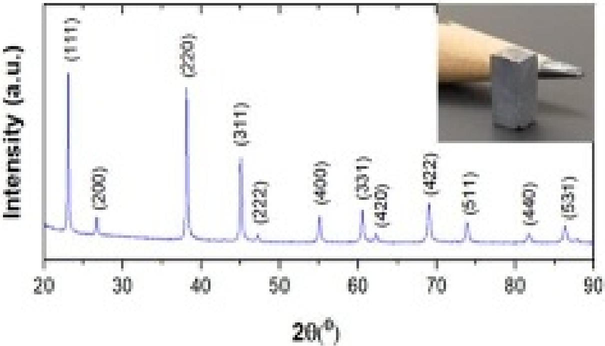

Intensity (a.u.)
(111)
(200)
(220)
(311)
(222)
(400)
(331)
(420)
(422)
(511)
(440)
(531)
20
30
40
50
60
70
80
90
2θ(°)

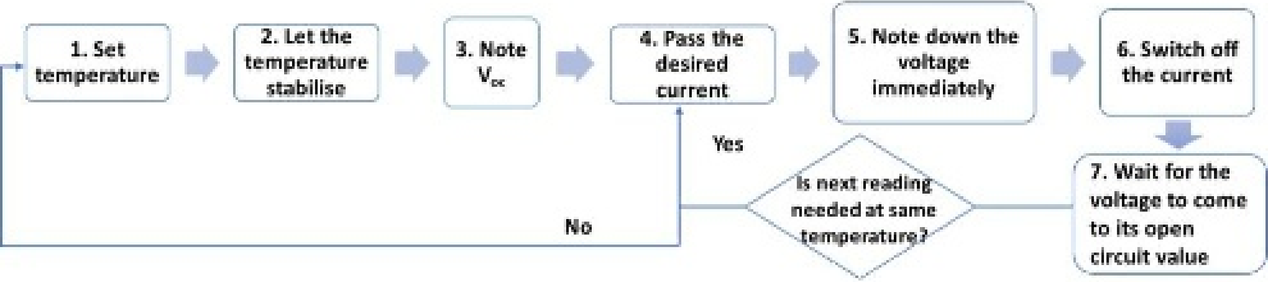
1. Set temperature
2. Let the temperature stabilise
3. Note V_{oc}
4. Pass the desired current
5. Note down the voltage immediately
6. Switch off the current
7. Wait for the voltage to come to its open circuit value
Is next reading needed at same temperature?
Yes
No

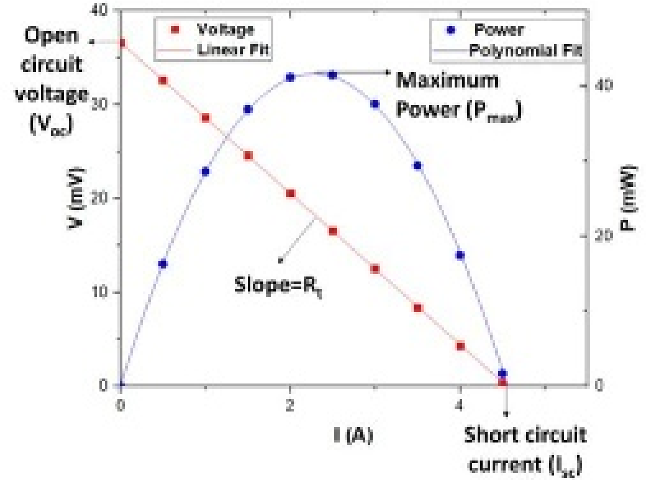

Open circuit voltage (V_{oc})
Voltage
Linear Fit
Power
Polynomial Fit
Maximum Power (P_{max})
Slope=R_i
V (mV)
P (mW)
I (A)
Short circuit current (I_{sc})
0
10
20
30
40
0
2
4
0
20
40

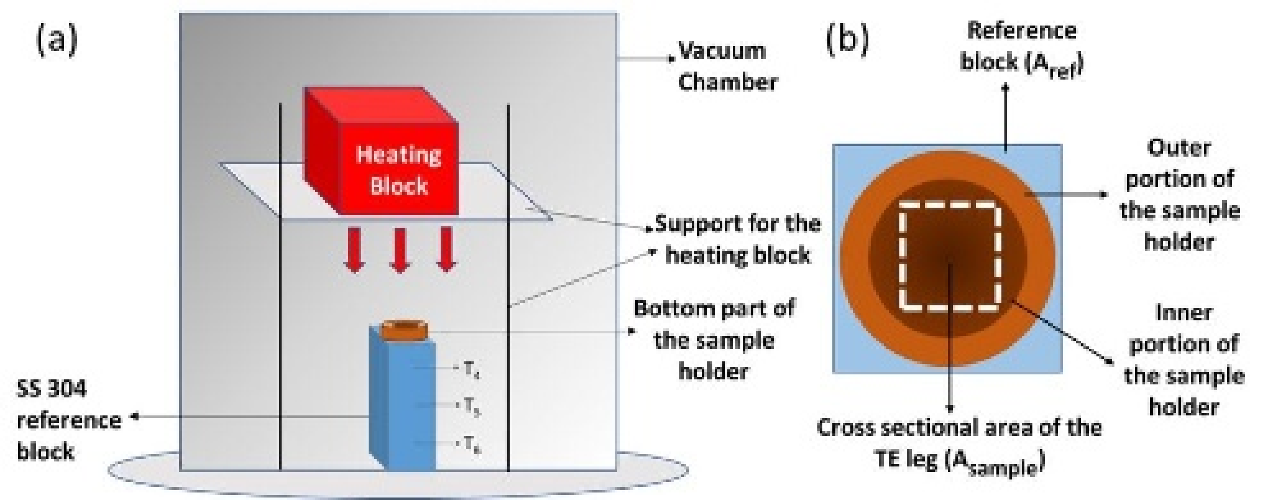
(a)
Vacuum Chamber
Heating Block
Support for the heating block
Bottom part of the sample holder
T_4
T_5
T_6
SS 304 reference block
(b)
Reference block (A_{ref})
Outer portion of the sample holder
Inner portion of the sample holder
Cross sectional area of the TE leg (A_{sample})

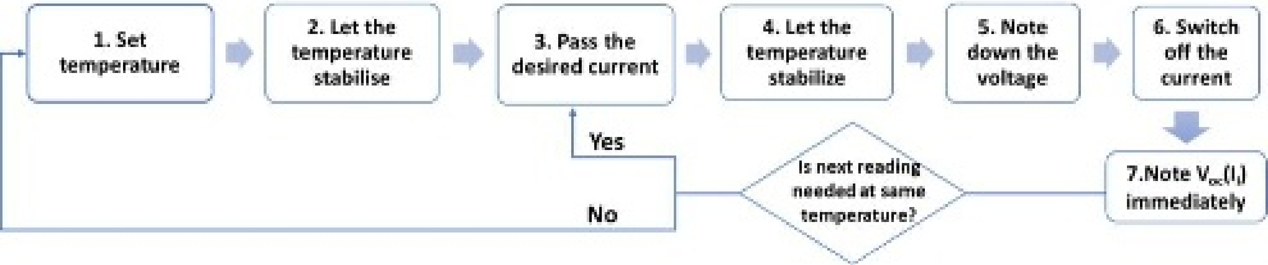
1. Set temperature
2. Let the temperature stabilise
3. Pass the desired current
4. Let the temperature stabilize
5. Note down the voltage
6. Switch off the current
7.Note $V_{oc}(I_i)$ immediately
Is next reading needed at same temperature?
Yes
No

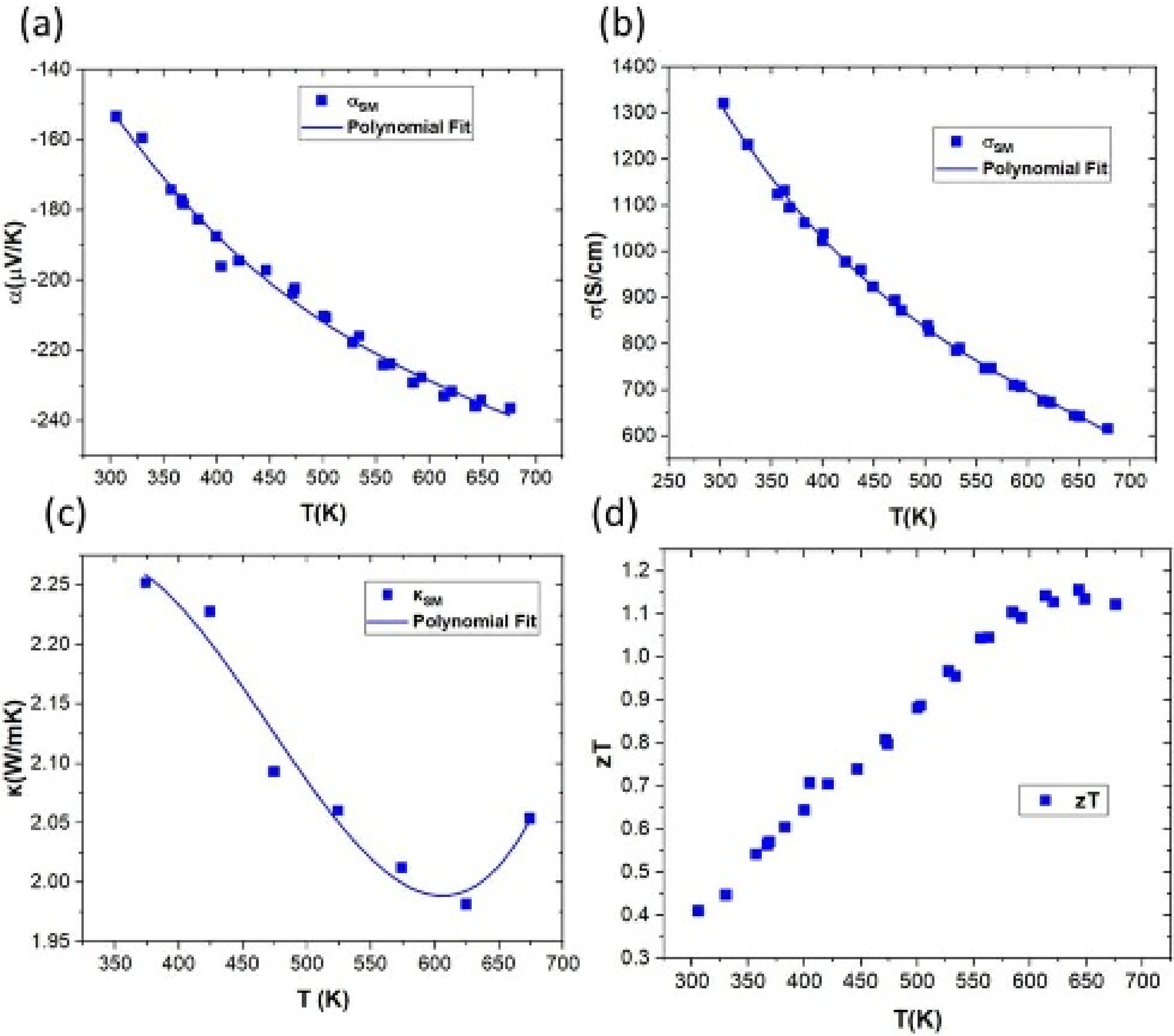
(a)
α(μV/K)
T(K)
α_SM
Polynomial Fit
(b)
σ(S/cm)
T(K)
σ_SM
Polynomial Fit
(c)
κ(W/mK)
T (K)
κ_SM
Polynomial Fit
(d)
zT
T(K)
zT

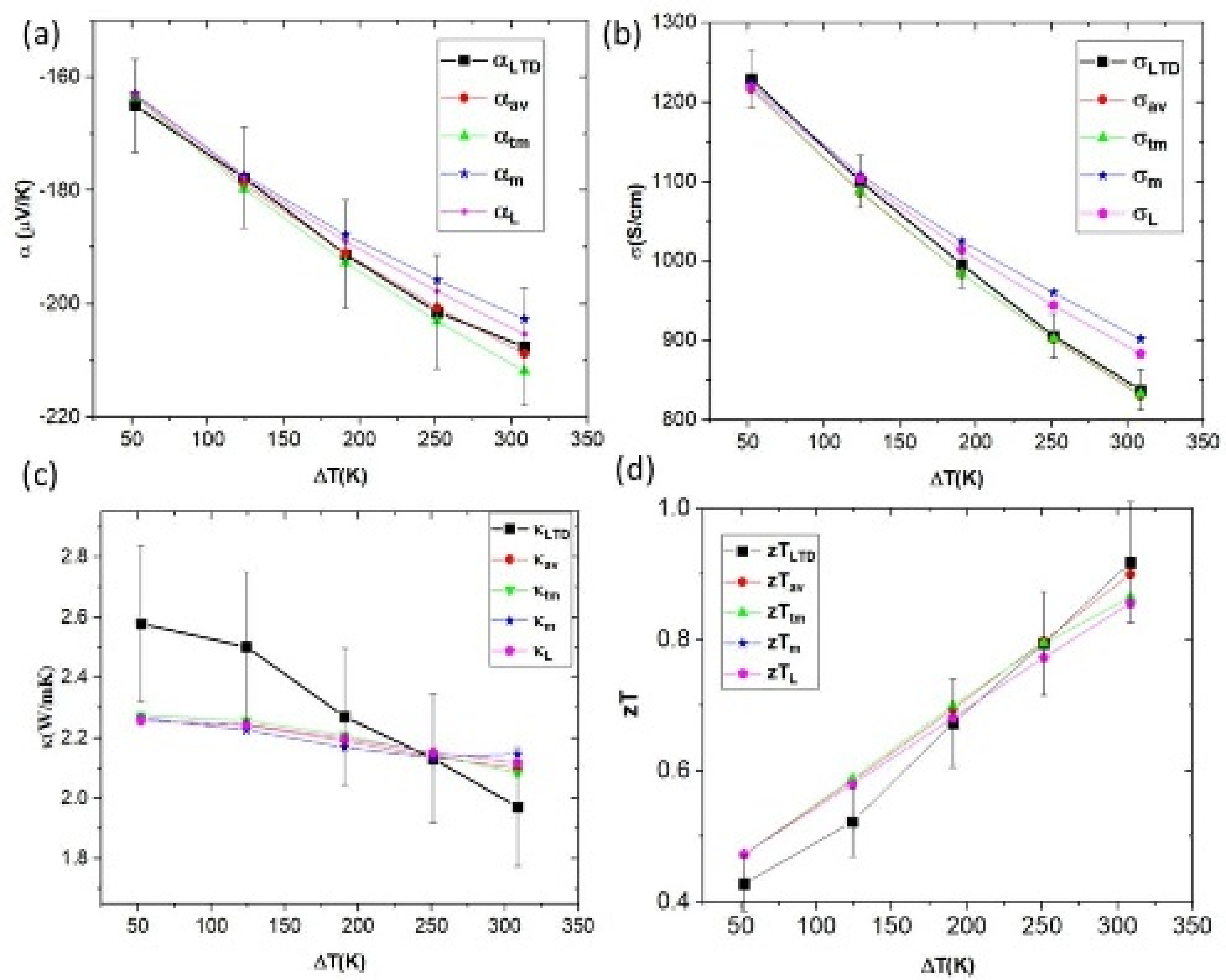

(a)
α_{LTD}
α_{av}
α_{tm}
α_{m}
α_{L}
α (μV/K)
-160
-180
-200
-220
50
100
150
200
250
300
350
ΔT(K)
(b)
σ_{LTD}
σ_{av}
σ_{tm}
σ_{m}
σ_{L}
σ(S/cm)
1300
1200
1100
1000
900
800
ΔT(K)
(c)
κ_{LTD}
κ_{av}
κ_{tm}
κ_{m}
κ_{L}
κ(W/mK)
2.8
2.6
2.4
2.2
2.0
1.8
ΔT(K)
(d)
zT_{LTD}
zT_{av}
zT_{tm}
zT_{m}
zT_{L}
zT
1.0
0.8
0.6
0.4
ΔT(K)

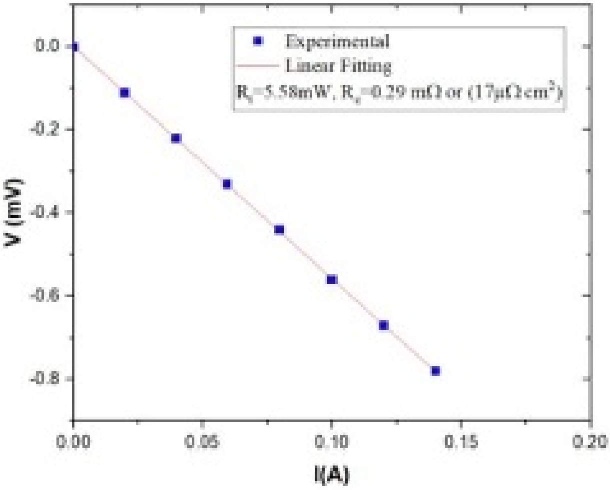
Experimental
Linear Fitting
R_t=5.58mW, R_c=0.29 mΩ or (17μΩ cm²)
V (mV)
I(A)
0.0
-0.2
-0.4
-0.6
-0.8
0.00
0.05
0.10
0.15
0.20

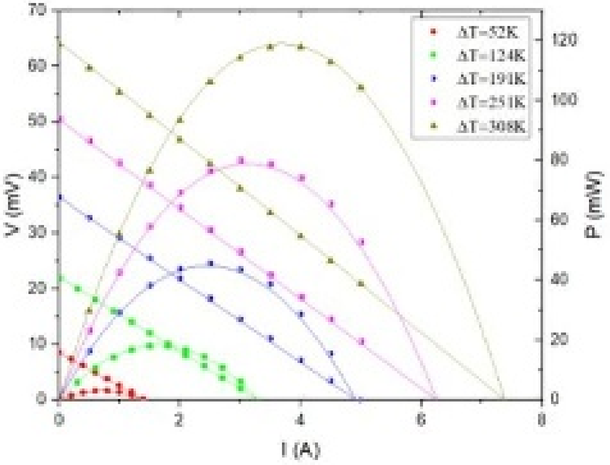

ΔT=52K
ΔT=124K
ΔT=191K
ΔT=251K
ΔT=308K
V (mV)
P (mW)
I (A)
0
10
20
30
40
50
60
70
0
2
4
6
8
0
20
40
60
80
100
120

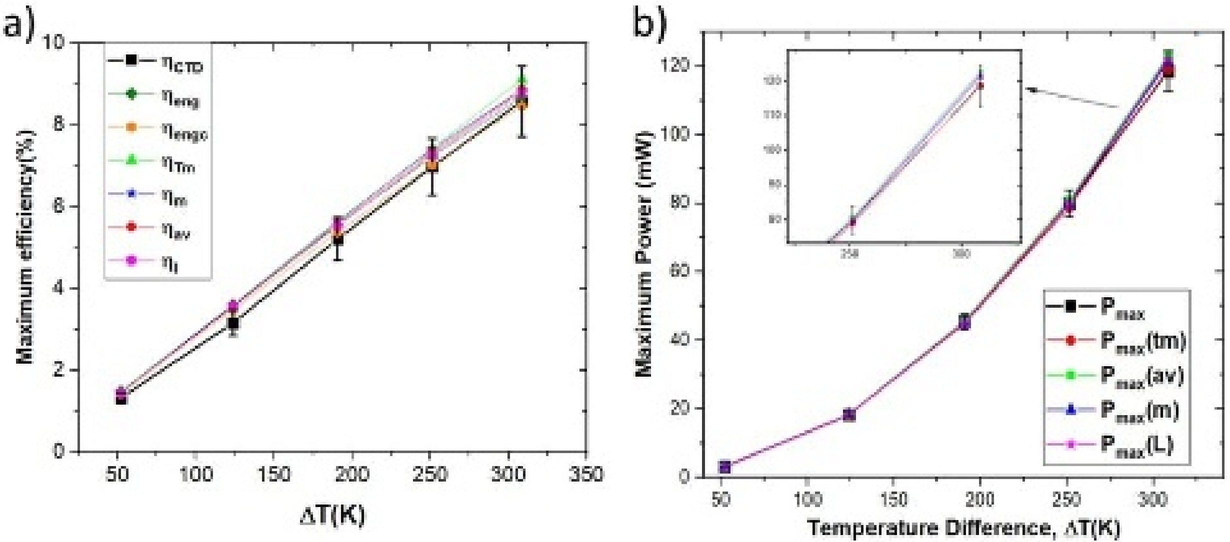
a)
Maximum efficiency(%)
ΔT(K)
ηCTD
ηeng
ηengc
ηTm
ηm
ηav
ηl
b)
Maximum Power (mW)
Temperature Difference, ΔT(K)
Pmax
Pmax(tm)
Pmax(av)
Pmax(m)
Pmax(L)

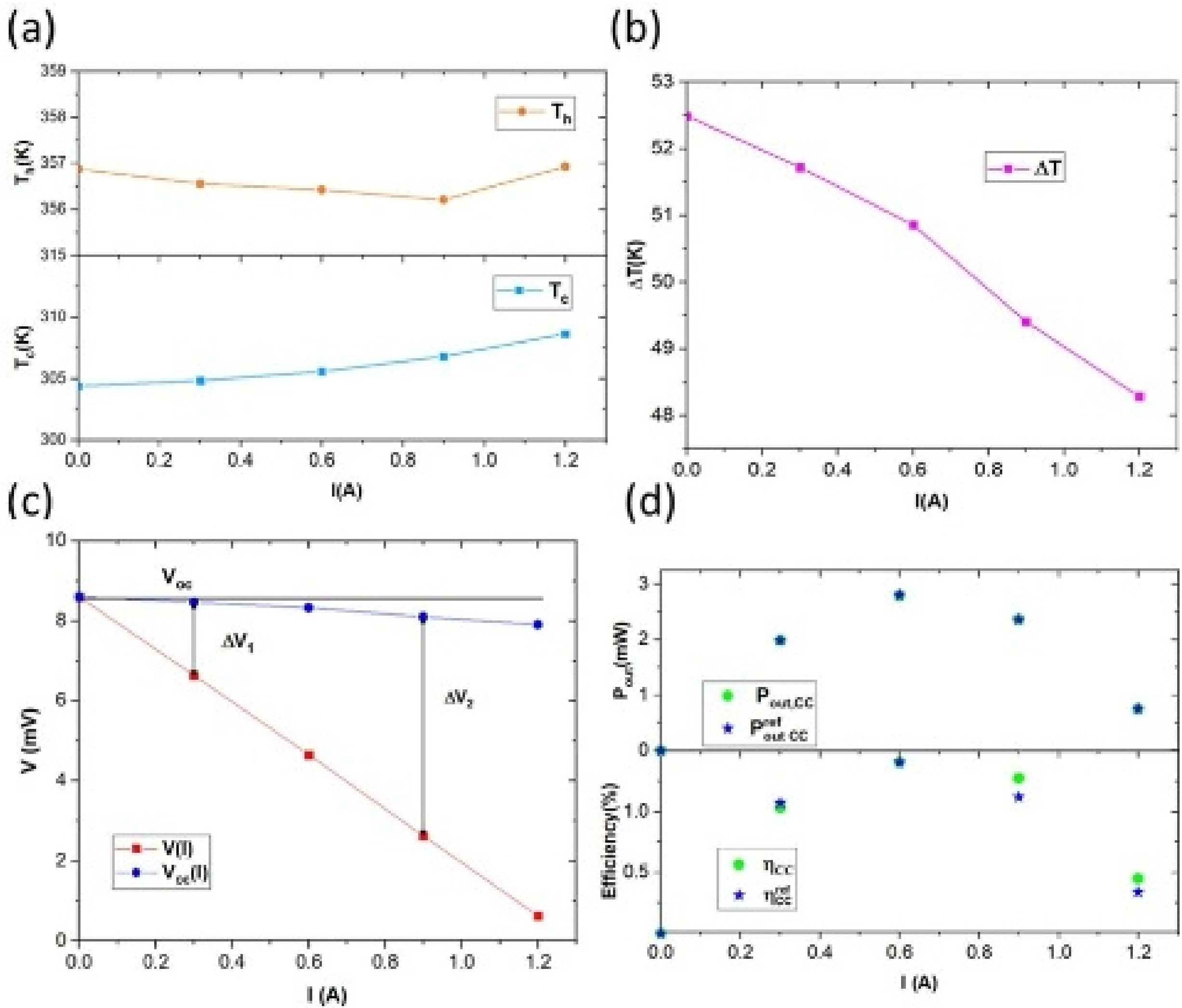

(a)
(b)
(c)
(d)
T_h
T_c
T_h(K)
T_c(K)
I(A)
ΔT
ΔT(K)
I(A)
V_oc
ΔV_1
ΔV_2
V(I)
V_oc(I)
V (mV)
I (A)
P_out,CC
P^ref_out,CC
P_out(mW)
η_CC
η^ref_CC
Efficiency(%)
I (A)

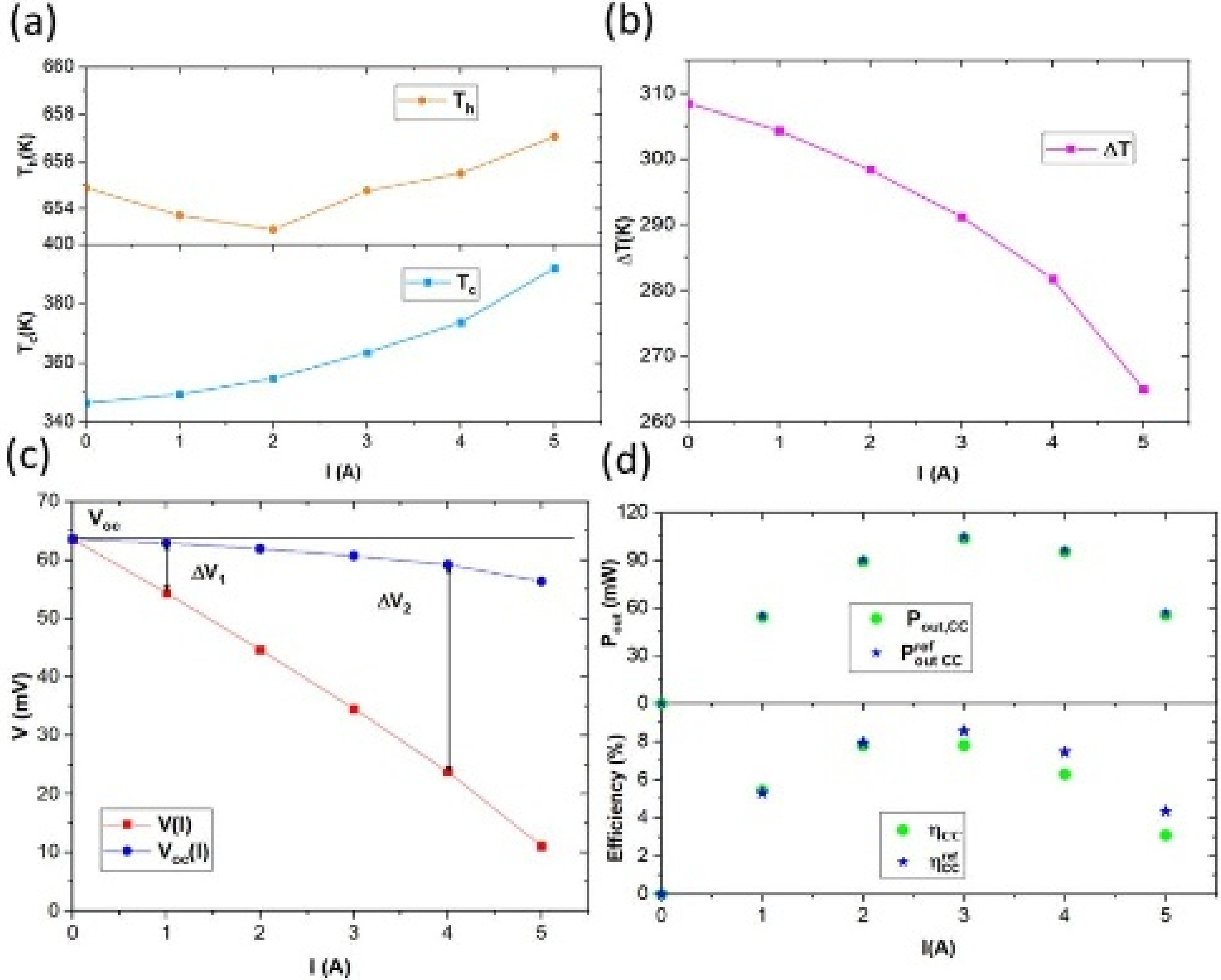

(a)
(b)
(c)
(d)
T_h
T_h(K)
T_c
T_c(K)
I (A)
ΔT
ΔT(K)
I (A)
V_{oc}
ΔV_1
ΔV_2
V(I)
V_{oc}(I)
V (mV)
I (A)
$P_{out,CC}$
$P^{ref}_{out\ CC}$
P_{out} (mW)
η_{CC}
η^{ref}_{CC}
Efficiency (%)
I(A)

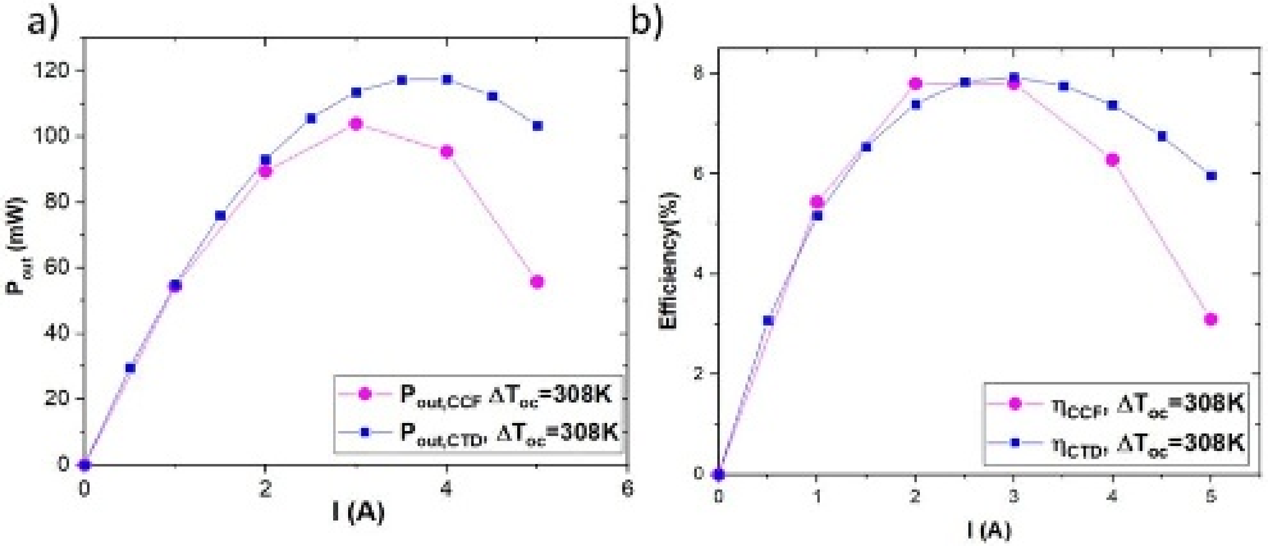
a)
b)
P_{out} (mW)
I (A)
$P_{out,CCF}$ ΔT_{oc}=308K
$P_{out,CTD}$, ΔT_{oc}=308K
Efficiency(%)
I (A)
η_{CCF}, ΔT_{oc}=308K
η_{CTD}, ΔT_{oc}=308K

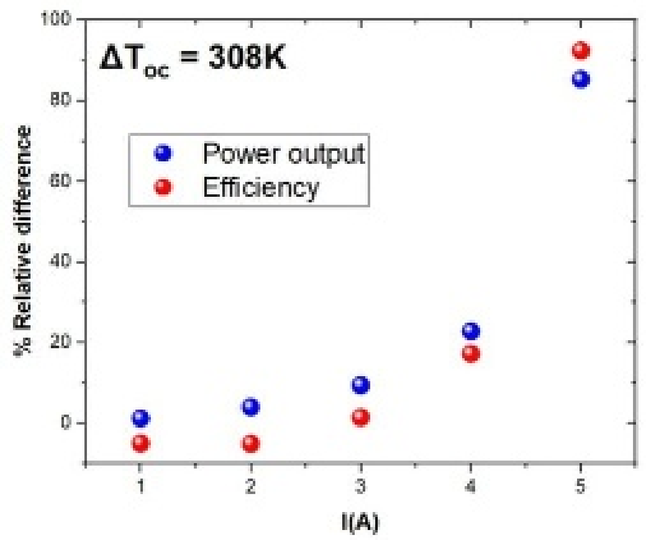

ΔT_{oc} = 308K
Power output
Efficiency
% Relative difference
I(A)
100
80
60
40
20
0
1
2
3
4
5

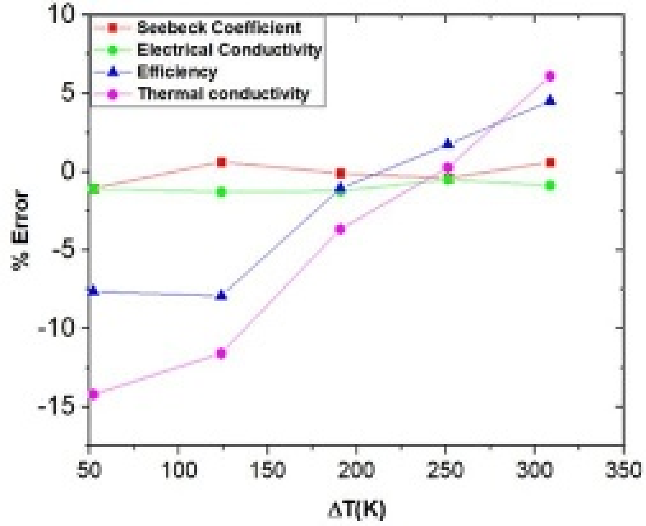
Seebeck Coefficient
Electrical Conductivity
Efficiency
Thermal conductivity
% Error
ΔT(K)
10
5
0
-5
-10
-15
50
100
150
200
250
300
350